Sirte University

Faculty of Science

Department of Chemistry

Utilizing a Cost-Effective Adsorbent Material Derived from Coconut Coir Fiber Modified with Hydrazone Compounds for Efficient Removal of Some Heavy Metals from Aqueous Environments

Student Name

SALWA AMER BELGASEM

Under Supervision

Professor Dr. Abdussalam Salhin Mohamed

Thesis Submitted in Partial Fulfilment of the Requirements for the Degree Master of Science in Chemistry

Academic Year 2024/2025

Declaration

I am Salwa A.Belgasem, and I confirm that the work in this thesis, unless Otherwise referenced is researcher`s own work, and has not been previously submitted to meet requirements of an award at this University or any other education or research institution, I furthermore, cede copyright of this thesis in favour of Sirt University.

Student name: Salwa Amer Belgasem.

Signature:

Date: 15/04/2025.

بِسْمِ اللَّهِ الرَّحْمَٰنِ الرَّحِيمِ

" وَعَلَّمَكَ مَا لَمْ تَكُن تَعْلَمُ ۚ وَكَانَ فَضْلُ ٱللَّهِ عَلَيْكَ عَظِيمًا"

صدق اللّهِ العلي العظيم

سورة النساء/ الآية (113)

DEDICATION

I dedicate this work to my wonderful parents, who have raised me to be the person I am today., to my siblings., whose support mean the world to me, and to my husband and my son, who inspire me every day.

ACKNOWLEDGEMENTS

First and foremost, I am deeply grateful to Almighty Allah for granting me the strength, perseverance, and knowledge to pursue and complete this research. I would like to express my profound and sincere gratitude to my research supervisor, Prof. Abdussalam Salhin, for giving me the opportunity to conduct this research and for providing invaluable guidance throughout the process. His vision, integrity, and motivation have been a constant source of inspiration. He has taught me the methodology for conducting research and presenting my work as clearly and effectively as possible. It has been a great honor to work and study under his supervision.

I am also deeply thankful to my fellow students, Seham Abdussalam, Mariam Ibrahim, and Sarah Abdullah, for their generous cooperation and assistance throughout this journey. My heartfelt thanks go to the Chemistry Department, its faculty members, and technicians, particularly Technician Wafaa, for their support.

I would also like to extend my gratitude to the Director of the Graduate Studies Department in the Faculty of Science, Prof. Hamid Younis, for providing all the necessary facilities to complete this work. Finally, I would like to acknowledge Ras Lanuf Company and Mr. Ali Al-Amari for their cooperation and assistance, which greatly contributed to the success of this research.

TABLE OF CONTENT

LIST OF TABLES

LIST OF FIGURES

LIST OF SCHEME

LIST OF SYMBOL AND ABBREVIATIONS

AAS	Atomic Absorption Spectrometer.
CF	Coconut Fiber (Coir).
°C	Degree Celsius.
C-L_1	Cellulose-DNPHACP.
C-L_2	Cellulose-DNPHACT.
C-L_3	Cellulose-DNPHB.
Conc.	Concentrate.
D	Distribution Coefficient.
DCM	Dichloromethane.
DMSO	Dimethyl Sulphoxide.
DNPH	2,4-Dinitrophenyl Hydrazine.
DNPHACP	2,4-Dinitrophenyl Hydrazone Acetophenone.
DNPHACT	2,4-Dinitrophenyl Hydrazone Acetaldehyde.
DNPHB	2,4-Dinitrophenyl Hydrazone Benzophenone.
DSC	Differential Scanning Calorimetry.
EtOH	Ethanol.
EtOAc	Ethyl Acetate.
FT-IR	Fourier Transform Infrared Spectrometer.
L min^{-1}	Liter per Minute.
mA	Milliampere.
MeOH	Methanol.
min	Minute.
mm	Millimeter.
M	Morality.
nm	Nanometer.
NMR	Nuclear Magnetic Resonance.
ppm	Part per Million.
Q	Capacity.
R/min	Revolutions per Minute.
SD	Standard Deviation.
SPE	Solid Phase Extraction.
UV/VIS	Ultraviolet-Visible Spectrometer.
XRD	X-Ray Diffraction.

ABSTRACT

In this study, 2,4-dinitrophenylhydrazine was subjected to a condensation reaction with acetophenone, acetaldehyde, and benzophenone, yielding hydrazone compounds. The ligands were isolated with satisfactory yields of 75%, 57%, and 85%, respectively. A sorbent material based on these hydrazone compounds was prepared by immobilizing the ligands onto cellulose extracted from coconut fiber. The percentage of cellulose obtained from 20 g of coconut fruit fiber powder reached 24.5% (4.9 g). The capability of the sorbent material for the extraction of Cu^{2+} was investigated using the batch method, and the extractants were analyzed by atomic absorption spectroscopy (AAS). The immobilized cellulose was employed as a stationary phase in solid phase extraction to isolate Cu^{2+} ions from aqueous solutions. Optimal conditions for effective extraction, including pH (5), contact time (10 min), and metal concentrations (Cu^{2+}, 0.05-100 ppm) and ligand (0.05×10^{-5} M), were determined. The results demonstrated that the sorbent-exhibited preferential selectivity for Cu^{2+} over other transition metals studied. The distribution coefficient (D) was found to be 0.999 mg/L. Adsorption kinetics followed a pseudo-second order model, confirming the efficiency of the process. The method was further tested for the extraction of Cu^{2+} ions from real samples, achieving reasonable recovery rates (>60%).

Chapter 1

INTRODUCTION

1.1 Hydrazone Compounds:

Hydrazone compounds, characterized by the presence of an azomethine (-NHN=C) moiety, are highly active compounds that have attracted significant research interest due to their straightforward synthetic routes [1]. These compounds are formed by the reaction of hydrazines with ketones or aldehydes, where the oxygen of the carbonyl group is replaced by the -NNH_2 functional group [2]. The general interaction between hydrazine and carbonyl compounds is illustrated in Scheme 1.

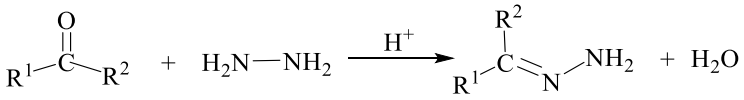

Scheme 1: General equation for the formation of hydrazone compounds. Where $R^1$and R^2 are aliphatic or aromatic organic groups [2].

These compounds have demonstrated significant antibacterial activity against pathogens, such as *Staphylococcus aureus*, *Escherichia coli*, and *Bacillus subtilis*, as well as cytotoxic effects on cancer cell lines like HeLa and MCF-7 [3]. Additionally, hydrazone compounds have been employed in the formation of metal complexes with diverse geometries and magnetic properties, further expanding their potential applications across various fields. The structural characterization of these compounds and their derivatives plays a crucial role in understanding their biological activities and therapeutic potentials [4]. Among the most widely utilized and commonly applied compounds in this field is 2,4-dinitrophenylhydrazine (DNPH) [5].

1.1.1 Hydrazone Applications:

Hydrazones represent a crucial category of analytical reagents used in the spectroscopic quantification of various metal ions in samples from food, environmental, pharmaceutical, and biological sources. Additionally, these compounds are employed in the analysis of organic substances such as glucose, carbonyl compounds, and estrogen in

matrices including blood, cell cultures, and pharmaceutical formulations [6]. They also serve as corrosion inhibitors for a range of metal ions, including Ni^{2+}, Cu^{2+}, Cr^{4+}, Si^{4+}, Mn^{2+}, S^{4+}, Cr^{6+}, Ti^{4+}, Co^{2+}, and Fe^{3+}, in both acidic and alkaline environments [6,7]. Furthermore, hydrazones are utilized in dyeing processes for materials like cotton and nylon, as well as in chemosensors, polymer initiation, sensitization, pH sensing for microbial detection, and wastewater treatment [6,8].

Hydrazones are capable of forming a variety of chromophoric complexes with metal ions such as Cu^{2+}, Mo^{6+}, Ni^{2+}, Pd^{2+}, Fe^{2+}, V^{5+}, U^{6+}, Al^{3+}, Th^{4+}, Hg^{2+}, Ru^{2+}, Pb^{2+}, Ti^{2+}, Cd^{2+}, Cr^{6+}, Au^{3+}, Co^{2+}, and Zr^{4+} [9,10]. Some chemical applications of hydrazones for metal ion selectivity are illustrated in Table 1.1.

Table 1.1: Some hydrazones compounds and their applications for metal ions selectivity.

No.	Ligand	Metal ion	Ref.
1	Isonitrosoacetophenone-2-aminobenzoyl hydrazone.	Cu^{2+},Ni^{2+}, Co^{2+}, Cr^{3+}, Hg^{2+}, Zn^{2+}, Cd^{2+}, Mn^{2+}	[11]
2	N-(benzoyl)-N-(salicylidine)-hydrazine.	Cu^{2+}	[12]
3	S-benzyl-b-N-(2- acetylpyrid-2-yl) methylene dinitro carbazate	Cu^{2+}	[13]
4	2, 6-diacetylpyridine bis ((DL-hydroxy (phenyl) acetic) hydrazone).	Cu^{2+},Ni^{2+},Fe^{2+}	[14]
5	7-Chloro-4-(o-hydroxybenzylidinehydrazone) quinoline	Cu^{2+}, Ni^{2+}, Co^{2+}, Fe^{3+}	[15]
6	6-Hydroxychromone-3-carbaldehyde benzoyl hydrazone	Ln^{3+}	[16]
7	2-Hydroxyaxetophenone 4- hydroxybenzoic acid hydrazone.	Cu^{2+}	[17]

Ref.: Reference

1.2 Heavy Metals:

The management of heavy metals poses a significant challenge due to their persistence and resistance to degradation in the environment [18]. Among these, Pb^{2+}, Cd^{2+}, Cu^{2+}, and Hg^{2+} are particularly hazardous, known for their toxic effects on both the environment and living organisms [18]. Prolonged exposure to these metals is associated with increased cancer rates and adverse effects on neurological, pulmonary, renal, integumentary, hepatic, and other organ systems. The molecular mechanisms underlying

their toxicity and carcinogenicity include DNA damage, oxidative stress induction, disruption of cellular respiration, interference with signal transduction pathways, and alterations in gene expression [19]. Various studies have explored effective methods for the removal and remediation of heavy metals [20-23]. Adsorption of these metal ions from aqueous solutions using adsorbents such as modified jute fiber and gelatin composites [24], kappa-carrageenan/cellulose hydrogels [25], acrylamide-grafted kolanut pod husk cellulose [26], alfa grass fibers [27], dendritic fibrous materials [28], and coconut fiber (CF) has shown promising results [29].

1.2.1 Copper:

The extensive use of copper in industrial processes can lead to elevated copper concentrations in the environment, potentially affecting drinking water quality. Copper ions exhibit biological activity, and their chelating properties, combined with their positive redox potential, facilitate their involvement in biological transport reactions. Cu^{2+} complexes are used as antiviral, antitumor, and antiinflammatory agents [30]. However, high concentrations of Cu^{2+} pose significant risks to environmental integrity and human health, causing severe damage to organs such as the liver, erythrocytes, heart, and brain [31]. Common techniques for copper determination include flame and electrothermal atomic absorption spectrometry (AAS), inductively coupled plasma mass spectrometry (ICP-MS), UV-visible spectrophotometry, anodic stripping voltammetry, and potentiometry using ion-selective electrodes [32]. However, direct quantification of trace copper in real samples is often hindered by interference from contaminants or insufficient sensitivity of the analytical methods [32]. Innovative techniques for copper extraction from environmental samples are crucial for identifying contamination levels and ensuring environmental safety. One such method is Solid-Phase Extraction (SPE) [33].

1.3 Solid Phase Extraction:

Solid-phase extraction (SPE) has gained significant recognition in analytical chemistry as an effective pre-concentration method for isolating trace metals [34]. SPE is preferred for extracting heavy metal ions from aqueous solutions due to its operational simplicity, lack of contaminants, high enrichment capability, efficient phase separation, time efficiency, and cost-effectiveness [35]. The efficacy of SPE depends on the adsorbent's characteristics, particularly its selectivity, detectability, sample throughput, and

reusability [36]. Fibrous materials have demonstrated notable adsorption capacities in various applications. Studies have shown that the adsorption effectiveness of botanical fibers increases after chemical modification [37]. Agricultural residues, composed primarily of cellulose, hemicellulose, and lignin [38], offer sorption capacities comparable to other natural sorbents, with the added advantages of low cost, high availability, and straightforward processing [29]. Recent studies have highlighted the significant adsorption capabilities of modified agricultural wastes, such as peanut shells and sawdust, for heavy metal ions like Cu^{2+}, Zn^{2+}, Ni^{2+}, Pb^{2+}, and Cr^{5+} [29].

Hydrazone-immobilized coconut fiber has emerged as an innovative adsorbent for metal ion extraction [37], with applications in the extraction of Au^{3+}, Cu^{2+}, and Ln^{3+} ions [39], as well as the removal of heavy metals such as Pb^{2+}, Cu^{2+}, and Zn^{2+} from wastewater [40].

1.3.1 Batch Method of Extraction:

The batch method is a common SPE technique in which a solid phase is used as an extractant to isolate a specific analyte from a solution. The solid material can then be analyzed directly or subjected to an elution process for analyte recovery [41]. Typically, a selective component is anchored onto a solid support such as silica, alumina, titanium dioxide, or a polymer, which serves as the solid phase in the batch method [42].

1.4 Coconut Palm:

The coconut palm, belonging to the *Palmaceae* family, is a tall, perennial evergreen tree. Its natural habitat is primarily associated with regions near the Pacific Ocean [43]. The fruit of the coconut palm consists of multiple layers (Figure 1.1), and its scientific classification is as follows:

Scientific Classification of Coconut Palm [44]**:**

- Kingdom: Vegetarian.
- Phylum: Angiosperms.
- Classification: Monocots.
- Order: Arecales.
- Family: Palmae.
- Tribe: Cocoeae.
- Gender: "Coconut".
- Scientific classification: *C. nucifera.*

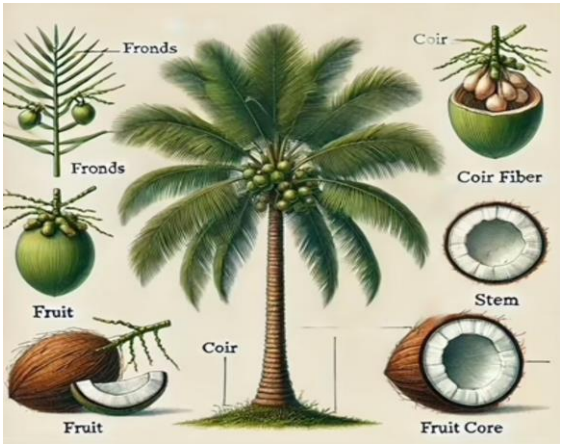

Figure 1.1: Main components of coconut palm [45]. (1) Fronds, (2) Fruit, (3) Coir (Fiber), (4) Stem, (5) Fruit core.

Coconut fiber (CF) has been extensively studied for its potential as an adsorbent in the removal of various metal ions from water [29]. The husk of the coconut, a byproduct that constitutes the mesocarp, represents approximately 33–35% of the whole husk [29]. The composition of coir fiber includes cellulose (38.01%), hemicellulose (2.30%), lignin (45.43%), and ash (1.21%). The significant cellulose content in coir fiber makes it a potential source for cellulose extraction [46].

Cellulose is a linear syndiotactic homopolymer with the molecular formula $(C_6H_{10}O_5)_n$, consisting of Danhydroglucopyranose units (glucose units). These units are inter connected via β-(1→4)-glycosidic bonds to form a dimer known as cellobiose, which serves as the fundamental building block of cellulose. Cellulose exhibits distinct physicochemical characteristics, including robust sorption capacity, making it a viable adsorbent in both its natural and modified forms [47]. Lignin is a highly complex, aromatic polyphenolic polymer with a cross-linked structure that binds the sugar molecules to the wood by chemical bonds. Lignin gives the plant rigidity, allowing it to grow taller. It also creates a physical barrier to the penetration and development of pathogens, and contributes to the natural protection of plants against some parasitic attacks. It constitutes about 15-40% of the plant's biomass [48] .While hemicellulose is a polysaccharide that constitutes about 20-40% of the biomass. It is a branched polymer consisting of a hexagonal monomer (C6: Hexosanes) such as (mannan and galactan) and a pentagonal monomer (C5: Pentosans) such as (xylan and araban). When chemically analyzed, we find it similar to mesamosa, but its hexagonal building unit is less stable compared to hemicellulose. Mesamosa has a generally non-morphic structure and relatively weak thermodynamic stability, as it tolerates fluidity and dissolves well in

alkalis [49]. Figure 1.2 presents the chemical structures of cellulose, hemicellulose, and cellulose fibers [50]. Table 1.2 illustrates some examples of cellulose immobilized with ligands and their applications for the extraction of metal ions.

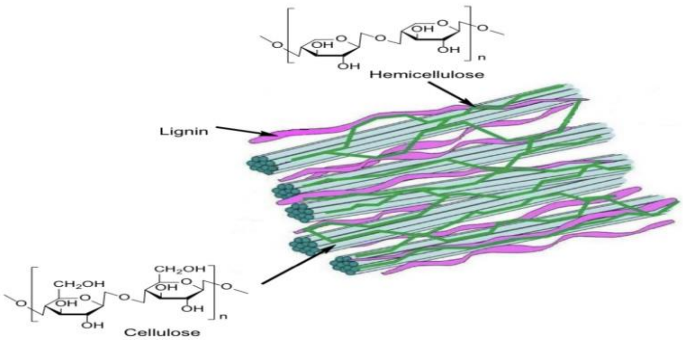

Figure 1.2: The chemical structure of cellulose, hemicellulose and Cellulose fibers [50].

Table 1.2: Examples of immobilized ligands on cellulose and their applications for metal ion extraction [51].

No.	Ligand	Source of Cellulose	Metal ions
1	Acrylamide (Amino) Ethylenediamine	Banana stalks, Cotton.	Hg^{2+}
2	Acrylonitrile	Bead	Cr^{3+}
3	Glycidyl methacrylate (Imidazole)	Grafting	Cu^{2+}, Ni^{2+}, Pb^{2+}
4	Acrylonitrile	Sunflower stalks	Cu^{2+}

1.5 Problem Statement:

Heavy metal contamination in water sources is a significant environmental and public health challenge worldwide. Industrial activities such as mining, metal processing, and chemical manufacturing release toxic metals, including copper, into water bodies, posing serious risks to ecosystems and human health. Traditional methods for removing these metals such as chemical precipitation, ion exchange, and membrane filtration are often costly, energy-intensive, and may generate secondary pollutants. This research addresses the need for an eco-friendly, cost-effective, and renewable solution by developing an adsorbent derived from coconut coir fiber. The study aims to provide a low-cost and efficient method for capturing and removing heavy metals from aqueous solutions.

1.6 Research Importance:

The research importance to achieve sustainability by developing an adsorbent material from a renewable source and using it to effectively remove heavy metals ions from aqueous solutions.

1.7 Research Aims:

1. Extraction of cellulose from coir fiber in an easy and cost-effective manner.
2. Synthesis of a hydrazone ligand as a complexation reagent.
3. Fabricate an adsorbent material based on the immobilization of synthesize ligand on cellulose.
4. Study of the extraction ability of the new adsorbent toward selected heavy metals.

Chapter 2

EXPERIMENTAL

2.1 Chemicals and Reagents:

Chemicals used in the study are listed in Table 2.1. All chemicals were used without further purification.

Table 2.1: Chemicals and reagents used in the study.

Chemical	Supplier
2,4-Dinitrophenylhydrazine,$C_6H_6N_4O_4$.	Riedel-de Haën.
Copper sulphate, Cu (SO_4).5H_2O.	Riedel-de Haën.
Lead nitrate, Pb (NO_3)$_2$.	Laboratory Reagent.
Ferric nitrate, Fe (NO_3)$_3$.6H_2O.	Laboratory Reagent.
Nickel nitrate, Ni (NO_3)$_2$.6H_2O.	Laboratory Reagent.
Acetaldehyde, CH_3CHO.	Riedel-de Haën.
Acetophenone, C_8H_8O.	BDH Chemical.
Benzophenone, $C_{13}H_{10}O$.	BDH Chemical.
Methanol, MeOH.	BDH Chemical.
Ethanol, EtOH.	Carlo Erba.
Dichloromethane, DCM.	Acros.
Dimethyl sulphoxide, DMSO.	Carlo Erba.
Ethyl acetate, EtOAc.	T-Baker Lab Chemicals.
Acetone, CH_3COCH_3.	Carlo Erba.
Nitric acid, HNO_3.	BDH Chemical.
Sulfuric acid, H_2SO_4.	T-Baker Lab Chemicals.
Hydrochloric acid, HCl.	BDH Chemical.
Acetic acid, CH_3COOH.	Timstar Laboratory.
Sodium hydroxide, NaOH.	Merck.
Sodium hypochlorate, NaClO.	Judy.

2.2 Apparatus:

Apparatus used in the study are listed in Table 2.2.

Table 2.2: Apparatus used in the study.

Apparatus	Supplier
Heater and motor.	Stuart.
Mill.	Hommer.
Filtration pump (RE3022C).	Stuart
Drying oven.	Bicasa.
Oven.	Muffle Furnace.
pH meter.	Thermo.
Reciprocating shaker.	Stuart.
UV/VIS Spectrophotometer.	Analytikjena.
AAS Spectrophotometer.	Shimadzu.
FT-IR Spectrometer.	Perkin Elmer.
DSC Analyzer.	Netzsch.

2.3 Preparation of Standard Solutions:

- A 7.5% solution of sodium hydroxide (NaOH) was prepared by dissolving 18.75g of NaOH in a 250 mL Erlenmeyer flask using distilled water.
- Different concentrations of DNPHB ($0.05–1\times10^{-5}$ M) were prepared by dissolving the appropriate amount (0.0002 g, 0.002 g, and 0.004 g) of the compound, in a 50 mL Erlenmeyer flask using DCM.

2.4 Preparation of Metal Ions Stock Solutions:

A 1000 ppm stock solution of transition metal ions (Cu^{2+}, Pb^{2+}, Ni^{2+}, and Fe^{3+}) was prepared by dissolving the appropriate amount of metal salts (Table 2.1) in a 2% HNO_3 solution.

2.5 Preparation of Raw Material:

The raw material was prepared following the general procedure described by Ashraf et al. [52]. Coconut fibers were collected, cut into small pieces, washed several times with tap water followed by distilled water, and dried in an oven at 80°C.

The fibers were ground using a mill (size 710 microns), washed again with distilled water, filtered, dried in the oven at 80°C, and stored in a desiccator. Figure 2.1 shows the coconut fibers before and after grinding.

(a) (b)

Figure 2.1: Coconut fibers (a) before and (b) after grinding.

2.5.1 Extraction of Cellulose from the Fibers [53]:

2.5.1.1 Removal of Wax:

This experiment was conducted using reflux distillation. A 20 g sample was placed in a 250 mL round-bottom flask, and an appropriate amount of a 1:1 mixture of acetone and ethanol was added. The flask was placed on a hot plate with magnetic stirring, and the mixture was heated at 60°C for 2 hours. The sample was then filtered, dried in an oven at 50°C for 15 minutes, and weighed. Figure 2.2 shows the filtration process after wax removal.

(a) (b)

Figure 2.2: (a) Filtration process after wax removal. (b) Sample after drying.

2.5.1.2 Removal of Hemicellulose and Lignin:

Reflux distillation was employed for this experiment. A portion of the sample obtained after wax removal was transferred to a 250 mL round-bottom flask. After attaching a condenser, 250 mL of a 7.5% NaOH solution was added. The flask was placed on a hot plate with magnetic stirring, and the mixture was heated at 60°C for 2 hours. The mixture was filtered, and the extraction process was repeated three times until a colorless (transparent) filtrate was obtained. The sample was washed with deionized water, dried in an oven at 80°C, weighed, and stored in a desiccator.

2.5.1.3 Bleaching:

The cellulose sample obtained from the previous step was placed in a 250 mL round-bottom flask and mixed with 250 mL of a 3.6% sodium hypochlorite solution. The flask was placed on a hot plate with magnetic stirring, and the mixture was heated at 90°C for 2 hours (Figure 2.3). The sample's color changed from brown to white. After filtering and washing with distilled water, the sample was dried at 80°C. The percentage of cellulose extracted was calculated using the following formula:

$$\text{Percentage of Cellulose} = \frac{\text{Callulose (g)}}{\text{Fiber (g)}} \times 100 \ldots\ldots\ldots\ldots\ldots\ldots\ldots\ldots\ldots\ldots\ldots\ldots \text{(1).}$$

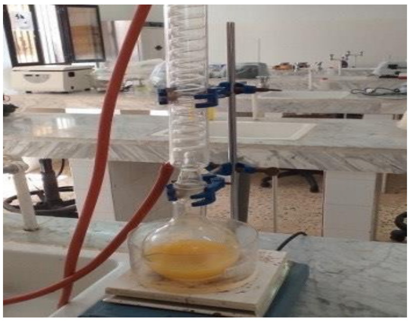

(a)

(b)

Figure 2.3: (a) Bleaching process using 3.6% sodium hypochlorate. (b) Cellulose sample after bleaching

2.6 Synthesis of Hydrazone Compounds:

All compounds were synthesized following the general procedure reported by Salhin et.al. [54], which involves the condensation of dinitrophenyl hydrazine (DNPH) with the appropriate aldehyde or ketone.

2.6.1 Synthesis of 2,4-Dinitrophenyl Hydrazone Acetophenone (DNPHACP, L_1).

A 0.59 g (0.003 M) of DNPH was dissolved in 4 mL of concentrated sulfuric acid in a 50 mL beaker, followed by the addition of 10 mL of ethanol. A 0.84 g (0.007 M) of acetophenone dissolved in 10 mL of ethanol was added to the beaker with stirring. An orange precipitate formed immediately. The product was filtered and air-dried, yielding 75%.

2.6.2 Synthesis of 2,4-Dinitrophenyl Hydrazone Acetaldehyde (DNPHACT, L_2).

A 0.59 g (0.003 M) of DNPH was dissolved in 4 mL of concentrated sulfuric acid in a 50 mL beaker, followed by the addition of 10 mL of ethanol. A 0.31 g (0.007 M) of acetaldehyde dissolved in 10 mL of ethanol was added to the beaker with stirring. A reddish-orange precipitate formed immediately. The product was filtered and air-dried, yielding 57%.

2.6.3 Synthesis of 2,4-Dinitrophenyl Hydrazone Benzophenone (DNPHB, L_3).

A 0.59 g (0.003 M) of DNPH was dissolved in 4 mL of concentrated sulfuric acid in a 50 mL beaker, followed by the addition of 10 mL of ethanol. A 1.275 g (0.007 M) of benzophenone dissolved in 10 mL of ethanol was added to the beaker with stirring. An orange precipitate formed immediately. The product was filtered and air-dried, yielding 85%.

2.7 Preparation of Adsorbent Material [52]:

The optimal solvent for immobilization was investigated, focusing on one that effectively dissolves moderately polar hydrazone compounds and is sufficiently volatile to aid in drying the loaded material. Three ligands (L_1, L_2, and L_3) were dissolved separately in various organic solvents (MeOH, EtOH, DMSO, EtOAc, DCM, and acetone). The immobilization process on ground cellulose fiber was carried out as follows:

1. In a 50 mL conical flask, 0.14 g (4.0×10^{-4} M) of L_1, 0.19 g (8.0×10^{-4} M) of L_2, and 0.002 g (0.5×10^{-5} M) of L_3 were weighed and each dissolved in 50 mL of DCM, then stirred for 30 minutes.
2. Next, 1.0 g of cellulose fiber was added to the ligand solution. This procedure was repeated with DMSO, MeOH, EtOH, EtOAc, and acetone.
3. Each mixture was sealed with paraffin film and allowed to stabilize for 24 hours.

4. After stabilization, the cellulose fibers were filtered, washed with distilled water, and dried in an oven at 60°C for 48 hours to remove residual solvent.
5. The amount of immobilized ligand on the cellulose fiber was calculated by UV/VIS analysis. The immobilized cellulose (Figure 2.4) was characterized by IR and DSC analysis (discussed in the next chapter).

Ligand	Solvent						
	x	1	2	3	4	5	6
L_1							
L_2							
L_3							

Figure 2.4: The prepared adsorbent material. Cellulose fiber before (x) and after immobilization with hydrazone ligands (L_1, L_2, L_3) in different organic solvents. : 1 = MeOH, 2 = EtOH, 3 = DMSO, 4 = EtOAc, 5 = DCM, 6 = acetone.

2.8 Extraction of Cu^{2+} (Batch Method) [55]**:**

A 10 mg sample of the adsorbent material (cellulose immobilized with L_3) was placed in a 20 mL glass vial. Then, 10 mL of a Cu^{2+} solution (1 ppm, pH 5) was added to the vial. The mixture was shaken mechanically (50 R/min) at room temperature for 10 minutes (Figure 2.5). After reaching equilibrium, the mixture was filtered, and the amount of unextracted Cu^{2+} ions in the filtrate was determined by AAS (Section 2.10). The amount of extracted Cu^{2+} was calculated by subtracting the remaining amount of Cu^{2+} from the initial amount.

Figure 2.5: Extraction process (Batch Method).

2.9 Preconcentration and Recovery of Cu^{2+} from Real Sample [55, 56]:

Water samples were collected from different locations on the Sirte University campus and the city center. The samples were filtered and stored in plastic bottles. Vegetable samples (tomatoes and potatoes) were collected from the city market. Washed several times with distilled water to remove dust, cut into small pieces, and dried in an oven at 80°C for 10 hours until a constant weight was achieved. The dried vegetables were ground and dried again at 105°C for 24 hours. A 0.50 g sample of the ash was mixed with 20 mL of HNO_3 (14 M) and heated until nearly dry. After cooling, the sample was diluted with distilled water to 50 mL and labeled as shown in Table 2.3.

Table 2.3: Real samples used in the study.

No.	Label	Sample	
		Type	Source
1	S_1	Water	Chemistry lab, Faculty of Medicine.
2	S_2	Water	Drinking water (SHAIMA).
3	S_3	Water	Water fountain in the downtown park.
4	S_4	Tomatoes	The city vegetable market.
5	S_5	Potatoes	The city vegetable market.

2.10 AAS Calibration Curve:

Table 2.4 presents the AAS instrumental operating conditions and data acquisition parameters, while Figure 2.6 shows the calibration curve for Cu^{2+} obtained from AAS.

Table 2.4: AAS instrumental operating conditions and data acquisition parameters.

Parameter	**Operating Condition**
Absorption wavelength (nm)	324.8
Lamp current (mA)	6
Burner height (mm)	7
Flow rate (L min^{-1})	1.8
Gas used	Acetylene flame, Air- C_2H_2
Number of replicate	3

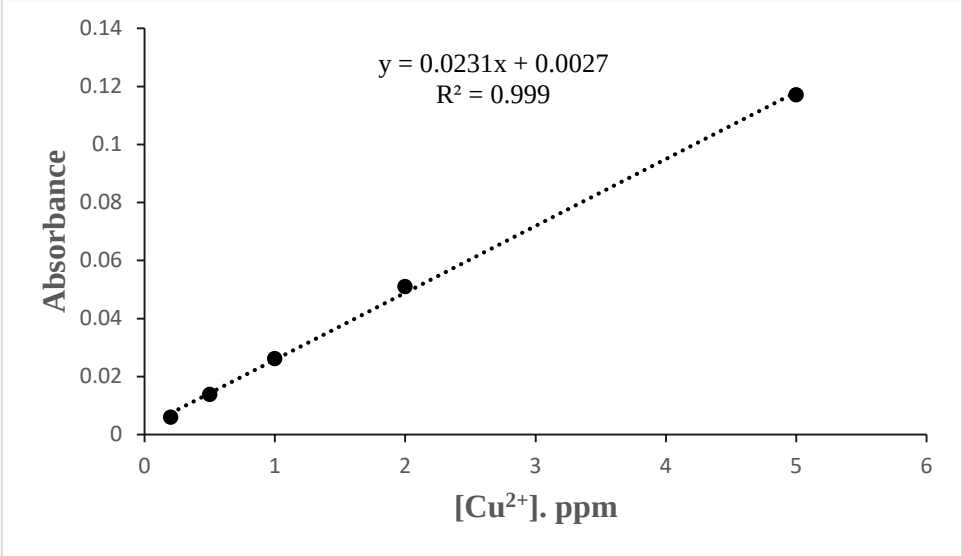

Figure 2.6: Calibration curve for Cu^{2+} using AAS.

Chapter 3

Results and Discussion

3.1 Extraction of Cellulose from Coconut Fiber:

The extraction of cellulose from coconut fiber was carried out using coconut fruit shells. During the extraction process, a noticeable color change was observed: the sample transitioned from brown (before treatment) to light brown (after removing hemicellulose and lignin) and finally to white (Figures 2.1, 2.2, and 2.3, respectively). The waxy substance was first removed by treating the fibers with a 1:1 mixture of acetone and ethanol. The fibers were then treated with a 7.5% sodium hydroxide solution to remove hemicellulose and lignin, followed by bleaching with a 3.6% sodium hypochlorite solution to obtain pure cellulose. The percentage of cellulose extracted from 20 g of coconut fruit was 24.5% (4.9 g). Table 3.1 summarizes the compositional analysis of the coconut fiber.

Table 3.1: Compositional analysis of cocount fiber.

Experiment	**Weight (g)**				
	Sample	**Waxy Substance**	**Lignin and Hemicellulose**	**Pure Cellulose**	**Other Materials**
1	20	5.0	9.4	4.0	1.6
2	20	6.0	7.7	5.0	1.3
3	20	5.0	7.9	5.6	1.5
Average (±SD) (%)		5.3 (±0.58) (26.5%)	8.3 (±0.93) (41.5%)	4.9(±0.81) (24.5%)	1.5(±0.61) (7.5%)

3.1.1 Characterization of Cellulose:

3.1.1.1 FT-IR Analysis

The FT-IR spectroscopic analysis of cellulose was conducted using a Perkin Elmer Frontier FT-IR Spectrometer with a Universal ATR Accessory (Single Bounce Diamond/ZnSe Crystal) at a scan accuracy of 4 cm^{-1}, covering a wavenumber range of 4000–400 cm^{-1}. Figure 3.1 shows a strong absorption band at 3334 cm^{-1}, indicating the presence of OH groups in cellulose, which contribute to its strength and hardness [57]. The signal at 2896 cm^{-1} corresponds to the vibration of C-H bonds in the hydrocarbon molecules of cellulose. Bands below 1500 cm^{-1} represent the vibrations of C-O and C-C bonds in the cellulose structure.

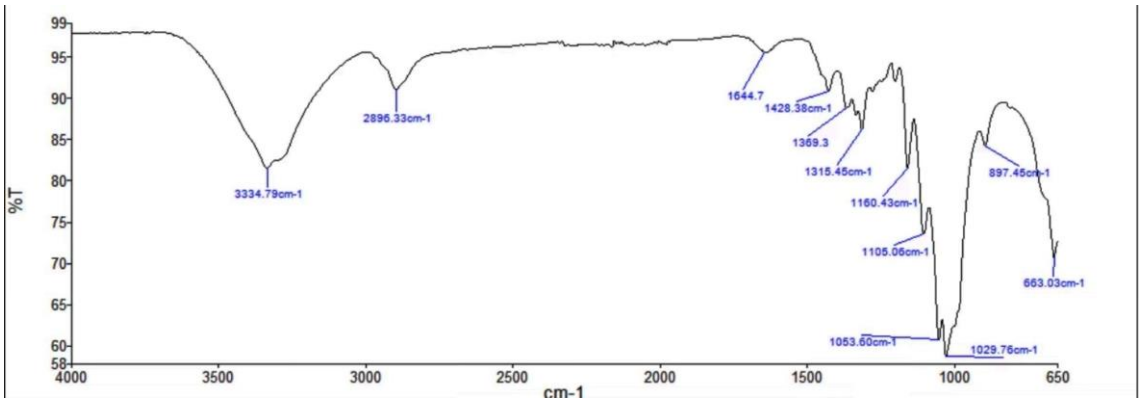

Figure 3.1: FT-IR spectrum of cellulose.

3.1.1.2 Differential Scanning Calorimetry (DSC).

Various analytical methods of analysis were used to determine the characterization properties of polymers. These methods include XRD, DSC, IR, and NMR [58]. The DSC method is considered the most widely used technique for characterizing polymers. The thermal behavior of cellulose (9 mg) was analyzed under a nitrogen atmosphere with a heating rate of 10°C/min from -35°C to 500°C. The thermogram (Figure 3.2) reveals several significant thermal peaks, including a broad endothermic peak at 87.7°C due to the loss of adsorbed water. The glass transition (T_g) and melting transition (T_m) were observed at 260–270°C (Table 3.2).

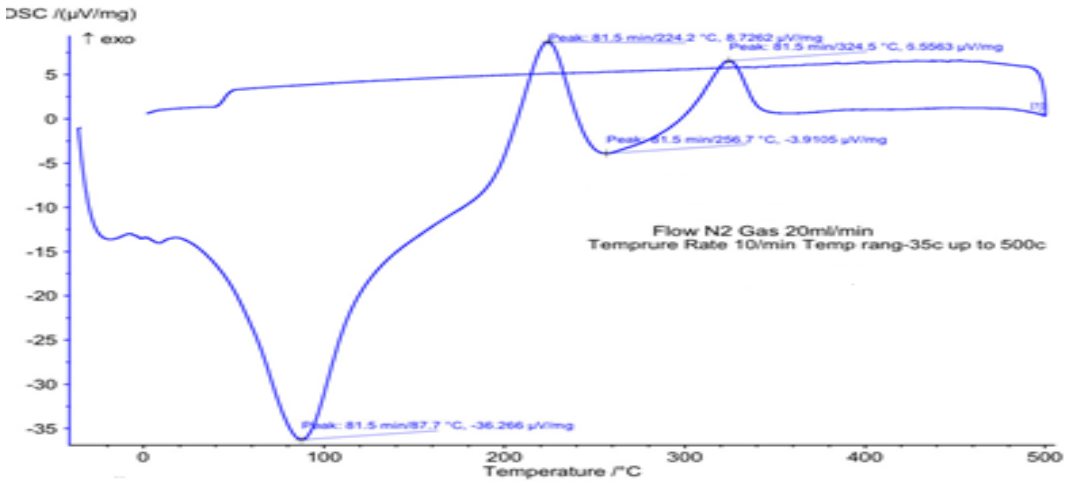

Figure 3.2: DSC curve of cellulose.

Table 3.2: Summary of Thermal Peaks of Cellulose.

Peaks Type	Temperature (°C)	Interpretation
Endothermic	85.4	Water loss
Exothermic	225.0	Crystal reorganization/Secondary crystallization
Exothermic	260-270	Melting transition
Exothermic	297.2	Structural transformation/Cross-linking
Exothermic	492.3	Thermal decomposition/Final degradation

3.2 Synthesis and Characterization of the Ligands

3.2.1 Synthesis of 2,4-Dinitrophenyl Hydrazone Acetophenone (DNPHACP), L_1.

L_1 was synthesized by condensing acetophenone with 2,4- dinitrophenylhydrazine [54]. The product, an orange powder (Figure 3.3), was characterized by FT-IR and DSC. The schematic diagram of the synthesis is illustrated in Scheme 2.

Figure 3.3: Orange powder of compound L_1.

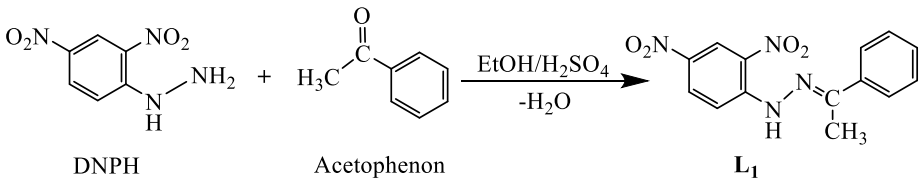

Scheme 2: Synthetic route for the synthesis of L_1.

3.2.1.1 FT-IR Analysis L_1.

The N-H vibration band was observed at 3304 cm^{-1} (Figure 3.4). C-H stretching vibrations were predominantly found in the range of 3118.7 cm^{-1}. Notably, the disappearance of the C=O band, characteristic of acetophenone, and its replacement by a strong band at 1614 cm^{-1} (corresponding to C=N stretching) confirmed the successful formation of L_1. The presence of NO_2 groups was verified through asymmetric and symmetric stretching vibrations at 1513 cm^{-1} and 1365 cm^{-1}, respectively. Additionally,

C-N vibration bands were identified in the region of 1218–1327 cm^{-1}, while aromatic ring vibrations were observed in the range of 1594–1582 cm^{-1} [57].

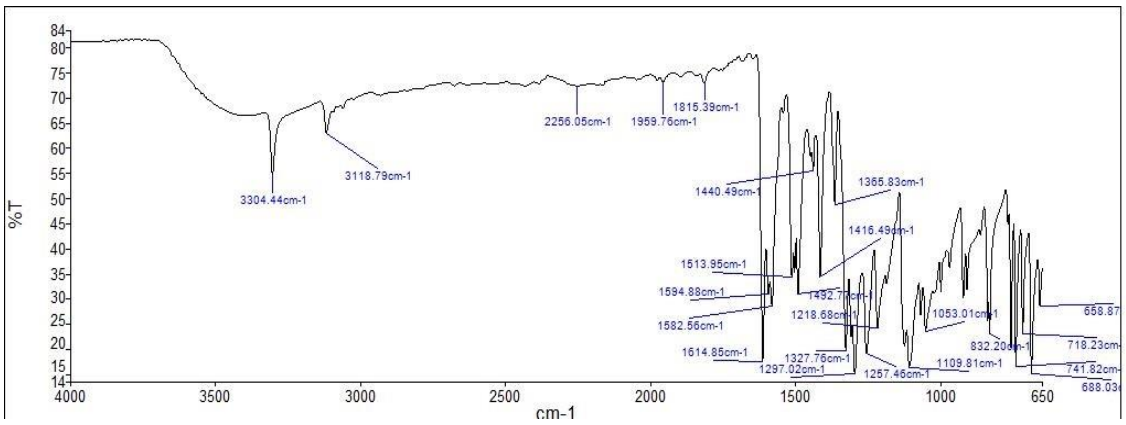

Figure 3.4: FT-IR spectrum of L_1.

3.2.1.2 Differential Scanning Calorimetry (DSC), L_1.

Figure 3.5 shows the DSC analysis of L_1, conducted with a sample mass of 9 mg under a nitrogen atmosphere. The temperature program ranged from -35°C to 500°C at a heating rate of 10°C/min. The thermogram reveals several significant thermal peaks, providing crucial insights into the material's thermal properties. Key phase transitions include:

- A peak at 102.8°C, representing the loss of residual solvents and potentially indicating a glass transition (T_g) of side groups.
- Peaks at 226.2°C and 275°C, corresponding to the melting point and the onset of thermal decomposition, respectively.

The compound demonstrates thermal stability up to 355°C. A summary of the thermal peaks is provided in Table 3.3.

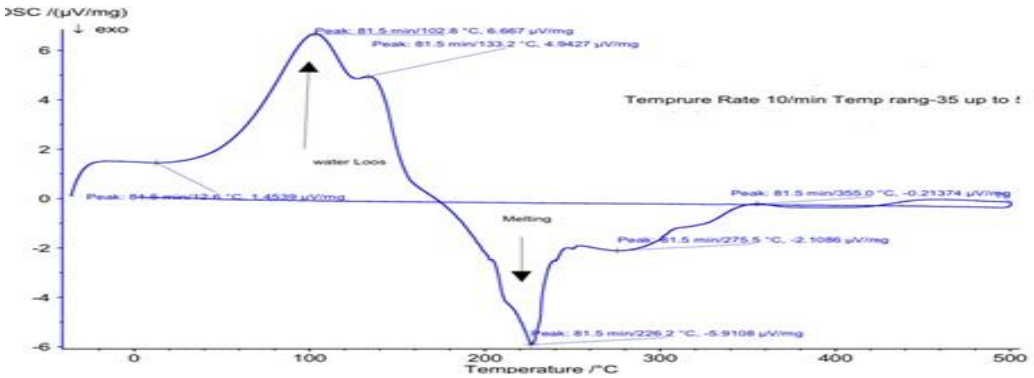

Figure 3.5: DSC curve of L_1.

Table 3.3: Summary of Thermal Peaks of L_1.

Peaks Type	Temperature (°C)	Interpretation
Exothermic	12.6	Initial phase transition
Exothermic	102.1	Primary water loss
Exothermic	133.2	Secondary water loss
Endothermic	226.2	Melting transition
Endothermic	273.5	Post-melt transition
Endothermic	355.0	High-temp transformation

3.2.2 Synthesis of 2,4-Dinitrophenyl Hydrazone Acetaldehyde (DNPHACT), L_2.

The synthetic route for L_2 involved the condensation of an equivalent ratio of acetaldehyde and 2,4-dinitrophenylhydrazine [54]. The resulting compound L_2, was obtained as a reddish-orange powder, as shown in Figure 3.6. The schematic diagram of the synthesis is illustrated in Scheme 3.

Figure 3.6: Reddish orange powder of compound L_2.

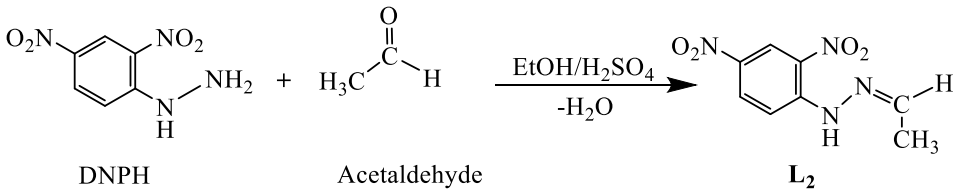

Scheme 3: Synthetic route for the synthesis of L_2.

3.2.2.1 FT-IR Analysis L_2.

The N-H vibration band was observed at 3290 cm^{-1} (Figure 3.7). C-H stretching vibrations were predominantly found in the range of 3057–3118.7 cm^{-1}. Notably, the disappearance of the C=O band, characteristic of acetaldehyde, and its replacement by a strong band at 1612 cm^{-1} (corresponding to C=N stretching) confirmed the successful formation of L_2. The presence of NO_2 groups was verified through asymmetric and symmetric stretching vibrations at 1509 cm^{-1} and 1307 cm^{-1}, respectively. Additionally,

C-N vibration bands were identified at 1264 cm^{-1}, while aromatic ring vibrations were observed in the range of 1590–1650 cm^{-1} [57].

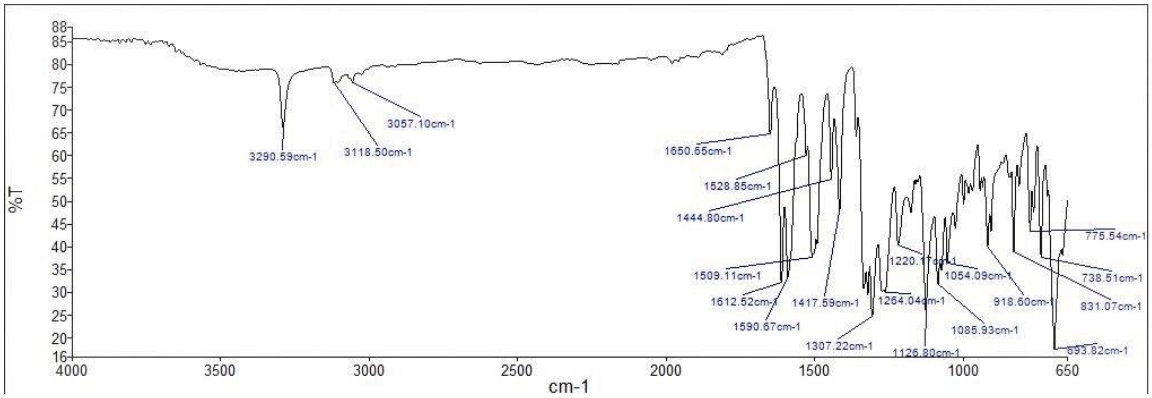

Figure 3.7: FT-IR spectrum of L_2.

3.2.2.2 Differential Scanning Calorimetry (DSC), L_2 .

Figure 3.8 shows the DSC analysis of L_2, conducted with a sample mass of 11 mg under a nitrogen atmosphere. The temperature program ranged from -35°C to 500°C at a heating rate of 10°C/min. The thermogram exhibits multiple thermal peaks, providing valuable insights into the material's thermal properties and phase transitions:

- A peak at 54.8°C, representing the loss of residual solvents and potentially indicating the crystallization process.
- A peak at 311.5°C, corresponding to the melting point.
- A peak at 430.3°C, marking the onset of thermal decomposition.

A summary of the thermal peaks is provided in Table 3.4.

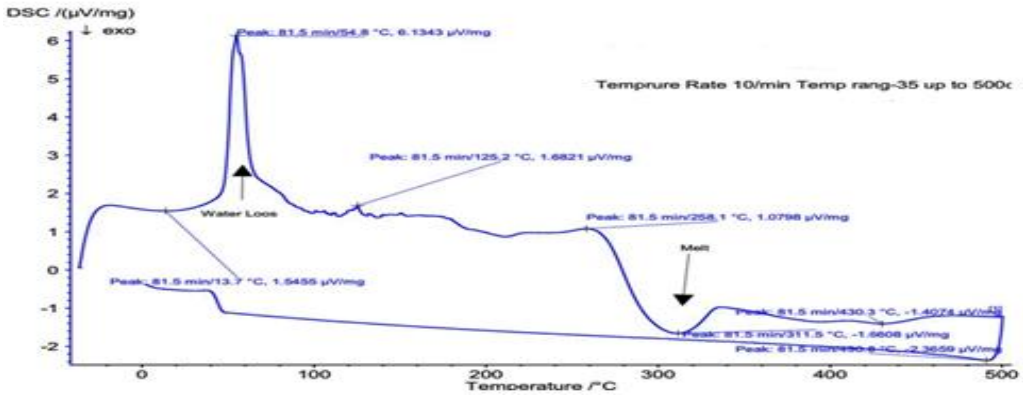

Figure 3.8: DSC curve of L_2.

Table 3.4: Summary of Thermal Peaks of L_2.

Peaks Type	Temperature (°C)	Interpretation
Exothermic	54.8	Water loss
Exothermic	132.0	Phase transformation
Exothermic	258.1	Minor structural change
Endothermic	311.5	Melting transition
Endothermic	453.2	High-temp transformation
Endothermic	494.8	Final decomposition

3.2.3 Synthesis of 2,4-Dinitrophenyl Hydrazone Benzophenone (DNPHB), L_3.

The synthetic route for L_3 involved the condensation of an equivalent ratio of benzophenone and 2,4-dinitrophenylhydrazine [54]. The resulting compound, L_3, was obtained as an orange powder, as shown in Figure 3.9. The schematic diagram of the synthesis is illustrated in Scheme 4.

Figure 3.9: Orange powder compound L_3.

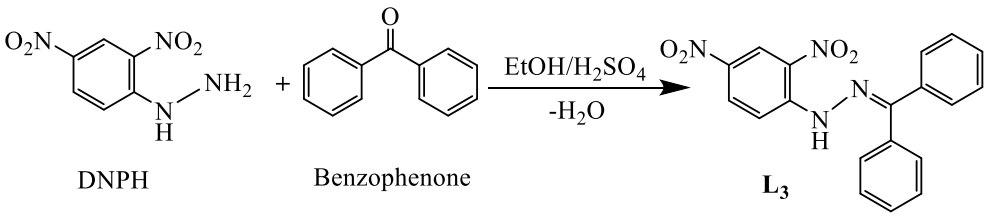

Scheme 4: Synthetic route for the synthesis of L_3.

3.2.3.1 FT-IR Analysis L_3.

The N-H vibration band was observed at 3288.7 cm^{-1} (Figure 3.10). C-H stretching vibrations were predominantly found in the range of 3057.2–3104.4 cm^{-1}. Notably, the disappearance of the C=O band, characteristic of benzophenone, and its replacement by a strong band at 1613 cm^{-1} (corresponding to C=N stretching) confirmed the successful formation of L_3. The presence of NO_2 groups was verified through asymmetric and

symmetric stretching vibrations at 1508 cm^{-1} and 1322 cm^{-1}, respectively. Additionally, C-N vibration bands were identified at 1257 cm^{-1}, while aromatic ring vibrations were observed in the range of 1590–1651 cm^{-1} [57]. A summary of the characteristic absorption bands for the synthesized ligands (L_1, L_2, and L_3) is provided in Table 3.5, along with their proposed assignments.

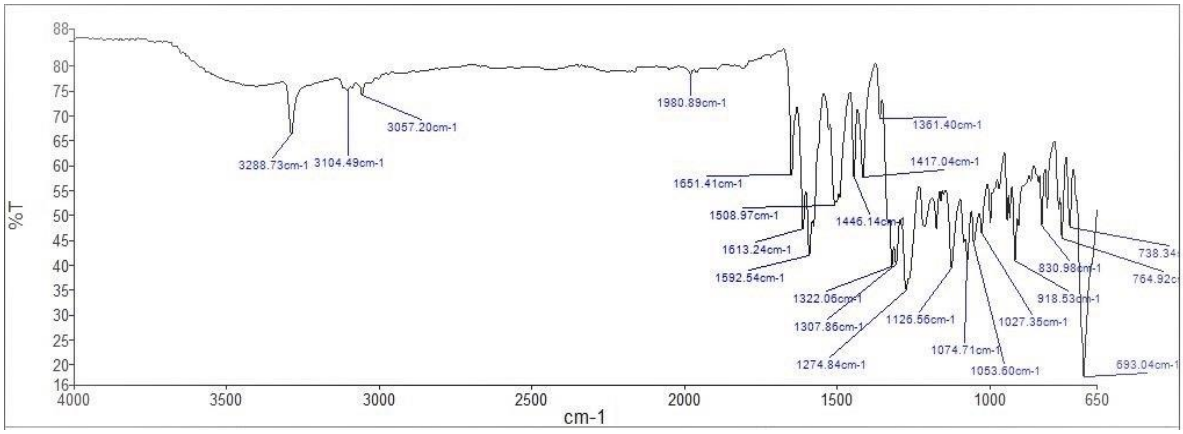

Figure 3.10: FT-IR spectrum of L_3.

Table 3.5: Selected FTIR stretching (cm^{-1}) for the synthesized compounds (L_1, L_2, and L_3).

Compound	N-H	C-H	C=O	C=N	NH_2	C-C	C-N	NO_2
L_1	3304	3118.7	-	1614	-	1594-1582	1218-1327	1513- 1365
L_2	3290	3057-3118.7	-	1612	-	1590-1650	1264	1509- 1307
L_3	3288.7	3057.2-3104..4	-	1613	-	1590-1651	1257	1508- 1322

3.2.3.2 Differential Scanning Calorimetry (DSC), L_3.

The DSC analysis was conducted on L_3 with a sample mass of (11 mg), using a heating rate of 10°C/min from -35°C up to 500°C was performed under a nitrogen atmosphere. The thermogram revealed several distinct thermal peaks, providing crucial insights into the compound's thermal properties and phase transitions (Figure 3.11). Primary dehydration process the most striking feature of the thermogram is an intense exothermic peak at 54.3°C with a remarkably high heat flow of 11.293 μV/mg. This peak, explicitly labeled as "Water Loss," represents a rapid and significant dehydration process. The sharpness and substantial magnitude of this peak suggest a highly ordered hydrate structure releasing its water molecules in a well-defined temperature range. This behavior indicates that water molecules might bound in specific crystallographic sites within the structure compound. Sequential Thermal process the DSC thermogram of L_3 shows a

multiple thermal transitions at various temperatures initial transition (13.7°C) an exothermic peak with a heat flow of 1.4033 μV/mg, possibly indicating an initial phase reorganization or crystal structure modification at low temperature. Intermediate Transition (167.1°C) a subtle exothermic event showing a heat flow of 1.14 μV/mg, which might represent a solid-solid phase transition or structural reorganization of the anhydrous material.

Melting region (274.0°C): A significant exothermic peak with a heat flow of 2.67 μV/mg, labeled as "Melting," was observed. The exothermic nature of this melting event is unusual and suggests concurrent crystallization or decomposition processes. High-temperature peak (326.5°C): An endothermic transition with a heat flow of 0.54817 μV/mg was detected, likely indicating thermal decomposition or structural breakdown. The thermal processes of compound L_3 are systematically summarized in Figure 3.11 and Table 3.6.

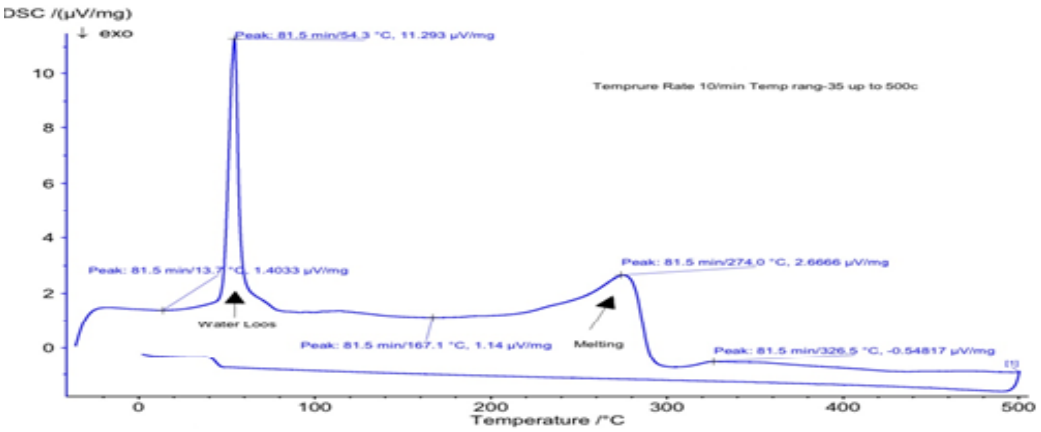

Figure 3.11: DSC curve of L_3.

Table 3.6: Summary of Thermal Peaks of L_3.

Peaks Type	Temperature (°C)	Interpretation
Exothermic	13.7	Initial phase transition
Exothermic	54.3	Major water loss
Exothermic	167.1	Phase transformation
Exothermic	274.0	Melting/Crystallization
Endothermic	326.5	Possible decomposition

3.3 Characterization of the Adsorbent Material:

3.3.1 FT-IR Analysis (C-L_1)

Figure 3.12 displays the IR spectra of L_1, cellulose fiber before ligand immobilization, and the adsorbent material (C-L_1). The spectra of C-L_1 and cellulose fiber showed comparable patterns. Key observations include:

- The C-O-C bond was identified by a broad and strong band between 1021-1053 cm^{-1}.
- The band at 662 cm^{-1} corresponds to C-O vibrations.
- Broad bands around 3337 cm^{-1} are attributed to OH stretching modes.

Notably, the C=N and NO_2 peaks, present in the spectrum of the free ligand (L_1), were absent in the spectra of cellulose and the adsorbent (C-L_1). This absence suggests that IR spectroscopy could not provide definitive evidence of L_1's presence in the cellulose matrix, likely due to the low concentration of the ligand in the cellulose network, as also reported by other researchers [55].

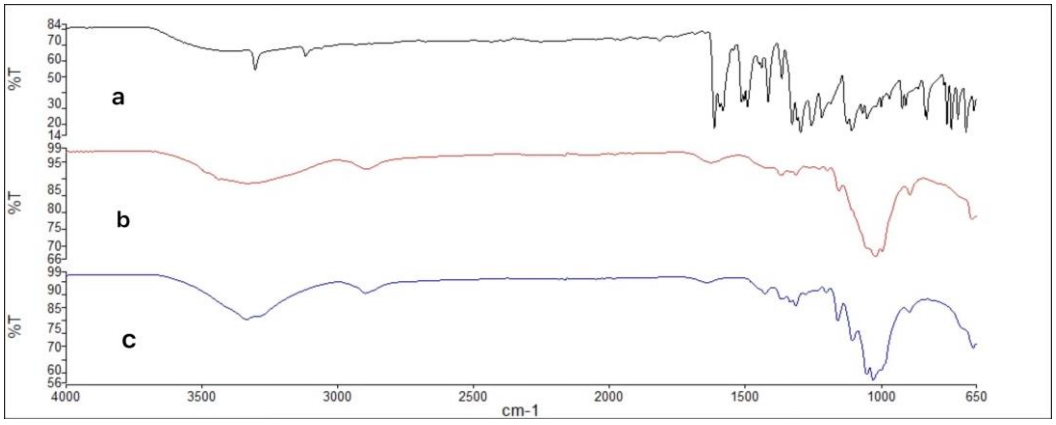

Figure 3.12: FT-IR spectrum of (a) L_1, (b) cellulose fiber and (c) C-L_1.

3.3.2 Differential Scanning Calorimetry (DSC).

The DSC analysis (Figure 3.13) was also conducted on the adsorbent material (C-L_1) with a sample mass of (6 mg), using a temperature program from -35°C to 500°C at a heating rate of 10°C/min was performed under a nitrogen atmosphere. The thermogram reveals several distinct thermal peaks that provide important information about the material's thermal properties and phase transitions. Initial and water loss peaks the thermogram shows an early exothermic event at -0.5°C, indicating an initial phase transition at low temperature. A prominent exothermic peak at 73.0°C, labeled as “Water Loss”, follows

this. The sharp and well-defined nature of this dehydration peak suggests a coordinated release of water molecules from specific crystallographic sites within the material's structure.

Melting and Phase Transitions: Interestingly, the material shows two closely spaced transitions in the intermediate temperature range: A transition at 140.5°C, a subsequent event at 166.7°C. Both these peaks are marked as "Melt" on the thermogram, suggesting a complex melting behavior possibly involving different crystalline phases or polymorphs. The final significant thermal peak High-Temperature Behavior occurs at 434.4°C with an endothermic heat flow of -1.3768 µV/mg, likely indicating thermal decomposition or structural breakdown of the material. Table 3.7 illustrated summary the thermal peaks of the adsorbent material (C-L_1).

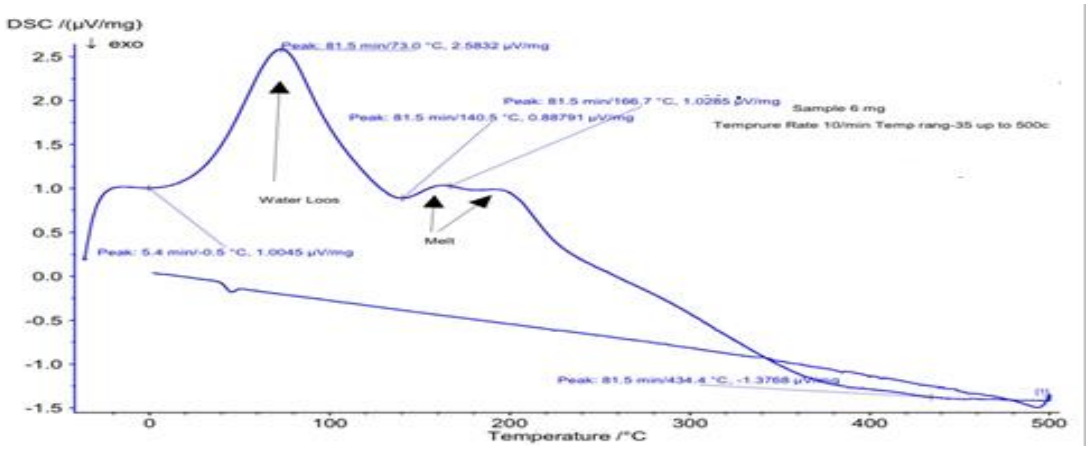

Figure 3.13: DSC curve of C-L_1.

Table 3.7: Summary of Thermal Peaks of C-L_1.

Peaks Type	Temperature (°C)	Heat Flow (µV/mg)	Interpretation
Exothermic	-0.5	1.0045	Initial phase transition
Exothermic	73.0	2.5832	Water loss
Exothermic	140.5	0.88791	First melting transition
Exothermic	166.7	1.0286	Second melting transition
Endothermic	434.4	-1.3768	Decomposition

3.3.3 FT-IR Analysis (C-L_2).

Figure 3.14 displays the IR spectra of L_2, cellulose fiber before ligand immobilization, and the adsorbent material (C-L_2). The spectra of C-L_2 and cellulose fiber showed comparable patterns. Key observations include:

- The C-O-C bond was identified by broad and strong band between 1029-1053 cm^{-1}.
- The band at 662 cm^{-1} corresponds to C-O vibrations.
- Broad bands around 3336 cm^{-1} are attributed to OH stretching modes.

Notably, the C=N and NO_2 peaks, present in the spectrum of the free ligand (L_2), were absent in the spectra of cellulose and the adsorbent (C-L_2). This absence suggests that IR spectroscopy could not provide definitive evidence of L_2's immobilization on the cellulose matrix, likely due to the low concentration of the ligand in the cellulose network, as also reported by other researchers [55] and discussed earlier in Section 3.3.1.

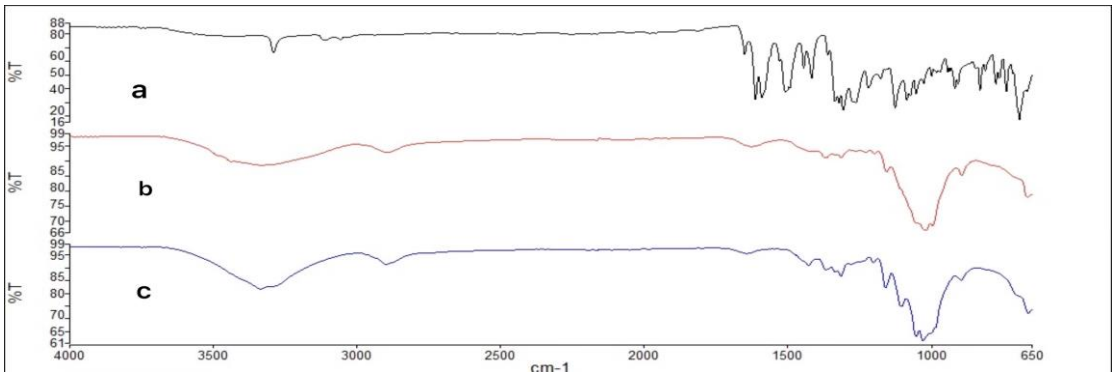

Figure 3.14: FT-IR spectra of (a) L_2, (b) cellulose fiber and (c) C-L_2.

3.3.4 Differential Scanning Calorimetry (DSC).

The DSC analysis of C-L_2 was conducted with a sample mass of 15 mg under a nitrogen atmosphere, using a heating rate of 10°C/min from -35°C to 500°C. The thermogram revealed several distinct thermal peaks, providing important insights into the material's thermal properties and phase transitions (Figure 3.15). Key Observations:

1. Melting Transition (T_m):
    - A prominent endothermic peak at 85.4°C (min: 52.0°C) likely corresponds to the melting transition of the crystalline domains. This peak suggests the presence of an ordered crystalline phase transitioning to a disordered state.
    - The sharpness and intensity of the peak indicate a relatively high degree of crystallinity in the sample.

2. Exothermic Transitions:
    - A small exothermic peak at 151.4°C, indicating a possible phase reorganization or secondary crystallization.
    - A more pronounced exothermic transition at 372.5°C, likely representing structural transformation or cross-linking.
    - A final exothermic peak at 497.3°C, marking the onset of thermal decomposition or final degradation.

A summary of the thermal peaks is provided in Table 3.8, illustrating the thermal behavior of the adsorbent material (C-L_2).

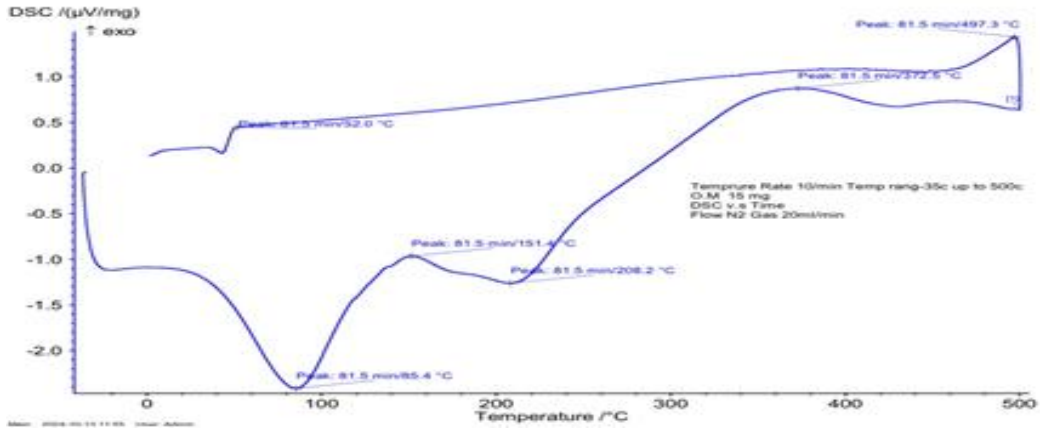

Figure 3.15: DSC curve of C-L_2.

Table 3.8: Summary of Thermal Peaks of C-L_2.

Peaks Type	Temperature (°C)	Interpretation
Endothermic	85.4	Melting transition (T_m)
Exothermic	151.4	Crystal reorganization/Secondary crystallization
Exothermic	372.5	Structural transformation/Cross-linking
Exothermic	497.3	Thermal decomposition/Final degradation

3.3.5 UV/VIS Analysis (C-L_3).

The adsorption immobilization of the ligand on cellulose fibers was measured at different concentrations (0.5 to 22 × 10^{-5} M) using a UV/Vis spectrophotometer (λ_{max} = 376 nm). The results demonstrated that the amount of ligand adsorbed on the cellulose increased proportionally with the ligand concentration, as shown by the linear relationship in Figure 3.16. The linear correlation between ligand concentration and absorbance confirms the effectiveness of the adsorption process.

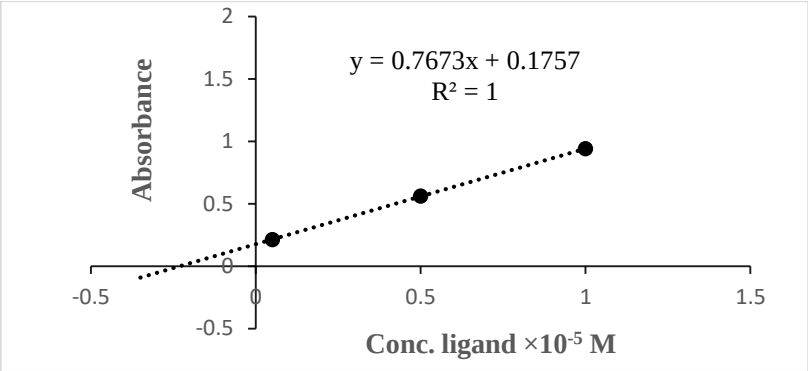

Figure 3.16: Liner curve of ligand concentration (0.05-1) $\times 10^{-5}$ M.

3.3.6 FT-IR Analysis (C-L_3).

Figure 3.17 displays the IR spectra of L_3, cellulose fiber before ligand immobilization, and the adsorbent material (C-L_3). The spectra of C-L_3 and cellulose fiber showed similar patterns. Key observations include:

- The C-O-C bond was identified by a broad, strong band between 1029-1052 cm^{-1}.
- The band at 662 cm^{-1} corresponds to C-O vibrations.
- Broad bands around 3336 cm^{-1} are attributed to OH stretching modes.

Notably, the C=N and NO_2 peaks, present in the spectrum of the free ligand (L_3), were absent in the spectra of cellulose and the adsorbent (C-L_3). This absence suggests that IR spectroscopy could not provide definitive evidence of L_3's presence in the cellulose matrix, likely due to the low concentration of the ligand in the cellulose network, as also reported by other researchers [55]. The IR spectra of cellulose fiber and immobilized cellulose (C-L_3) showed no significant differences (Figure 3.17 b and c).

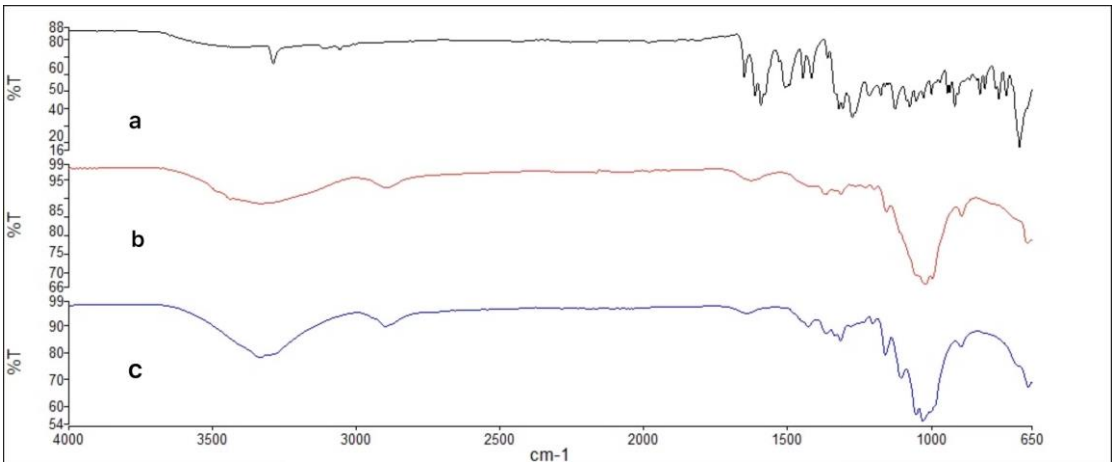

Figure 3.17: FT-IR spectra of (a) L_3, (b) cellulose fiber and (c) C-L_3.

3.3.7 Differential Scanning Calorimetry (DSC)

Figure 3.18 shows the DSC analysis of C-L_3 (11 mg), conducted under a nitrogen atmosphere using a temperature program from -35°C to 500°C at a heating rate of 10°C/min. The thermogram reveals several distinct thermal peaks, providing important insights into the material's thermal properties and phase transitions. Key Observations:

1. Primary Dehydration Process:
   - A prominent exothermic peak at 100.6°C (heat flow: 2.9603 μV/mg), labeled as "Water Loss," indicates the release of bound water molecules.
   - The sharpness and intensity of the peak suggest a coordinated release from specific crystallographic sites within the material's structure [59].
2. Thermal Transitions:
   - An initial exothermic peak at 19.9°C (heat flow: 1.1986 μV/mg) likely represents phase reorganization or structural modification.
   - An endothermic peak at 223.5°C (heat flow: - 0.87556 μV/mg) suggests a phase transition.
   - A transition at 257.1°C (heat flow: 0.20839 μV/mg) may indicate further structural reorganization.
3. Melting and Decomposition:
   - A melting transition at 326.1°C (heat flow: - 0.83133 μV/mg) was observed.
   - A final endothermic peak at 455.0°C (heat flow: - 0.85675 μV/mg) likely marks the onset of thermal decomposition.

A systematic summary of the thermal properties is provided in Table 3.9.

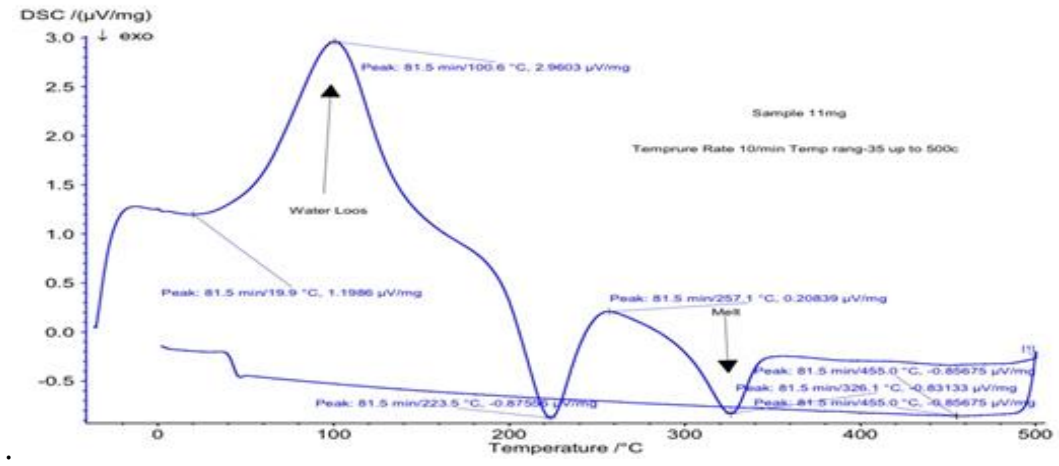

Figure 3.18: DSC curve of C-L_3.

Table 3.9: Summary of Thermal Peaks of C-L_3.

Peaks Type	Temperature (°C)	Heat Flow (µV/mg)	Interpretation
Exothermic	19.9	1.1986	Initial reorganization
Exothermic	100.6	2.9603	Water loss
Endothermic	223.5	-0.87556	Phase transition
Exothermic	257.1	0.20839	Crystallization
Endothermic	326.1	-0.83133	Melting
Endothermic	455.0	-0.85675	Decomposition

3.4 Solid-Phase Extraction of $Cu^{2+}$and Pb^{2+}Using adsorbent materials, (Batch Method):

The adsorbent materials (C-L_1, C-L_2, and C-L_3) were used for the extraction of Cu^{2+} and Pb^{2+} from aqueous medium. Results showed that C-L_3 adsorbent material had a better extraction ability towards Cu^{2+}. Figure 3.19 shows the effect of adsorbent material (C-L_1, C-L_2 and C-L_3) on the extraction of Cu^{2+} and Pb^{2+} from aqueous solution. The percentage of extraction was calculated using the formula given below [58]:

$$\%E = \frac{C_0 - Ce}{C_0} \times 100 \quad \ldots\ldots\ldots\ldots\ldots\ldots\ldots\ldots\ldots\ldots\ldots\ldots \quad (2).$$

- C_0 = Initial metal ion concentration in solution (mg/L).
- C_e = Equilibrium metal ion concentration in solution (mg/L).

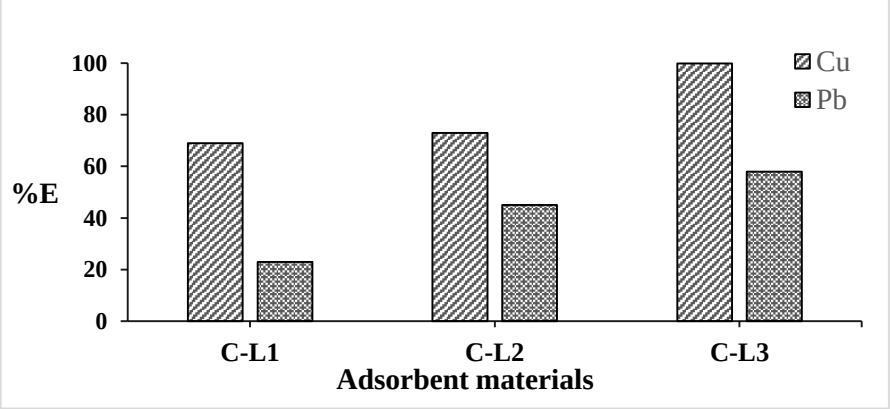

Figure 3.19: Effect of adsorbent material (C-L_1, C-L_2, C-L_3) on the extraction of Cu^{2+} and Pb^{2+}. pH 5 and contact time 60 min using batch method.

The number of milligram of Cu^{2+} adsorbed (Q, mg g^{-1}) per gram of sorbent [61, 62] was calculated to characterize the exchange process between the two phases (solid/liquid). The value was calculated using the following equation:

$$Q = \frac{(C_0 - Ce)V}{m} \quad \ldots\ldots\ldots\ldots\ldots\ldots\ldots\ldots\ldots\ldots\ldots\ldots\ldots\ldots\ldots (3).$$

Where (V) is the volume of the solution (L) and (m) is the mass of the sorbent material in grams. The C-L_3 adsorbent material demonstrated superior selectivity for Cu^{2+} over Pb^{2+} compared to the other adsorbents studied (Figure 3.20). As a result, further investigations were conducted to explore the extraction capabilities of C-L_3 for Cu^{2+}.

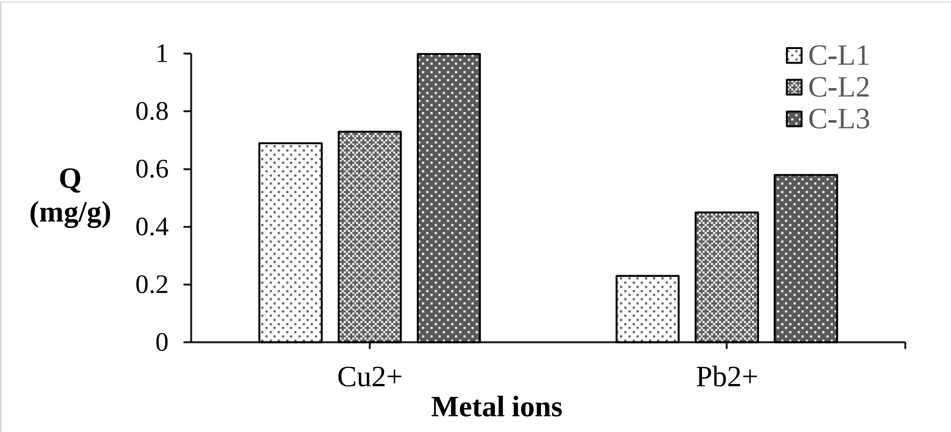

Figure 3.20: The total capacity (Q) of the adsorbent material (C-L_1, C-L_2 and C-L_3) on the extraction of Cu^{2+} and Pb^{2+}. pH 5 and contact time 60 min using batch method.

Figure 3.21 shows a comparison of the FT-IR spectra of C-L_3 before and after extraction with Cu^{2+}. However, as mentioned earlier (Section 3.3.5), FT-IR analysis did not provide clear evidence of complexation between the adsorbent and Cu^{2+}. The DSC spectra of C-L_3 after Cu^{2+} extraction (Figure 3.22) revealed a significant reduction in the intensity of peaks associated with the organic compound compared to the spectrum of C-L_3 before extraction. This reduction suggests that a substantial portion of the compound reacted with copper. The absence of certain peaks further supports this observation, likely due to interactions between copper and the ligand on the adsorbent.

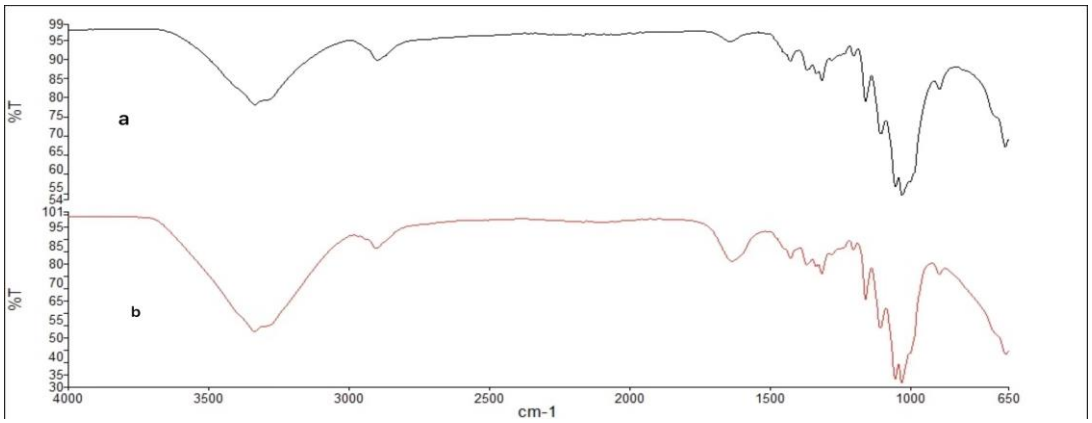

Figure 3.21: FT-IR spectrum of C-L_3 (a) before and (b) after extraction of Cu^{2+} from aqueous solution (pH 5).

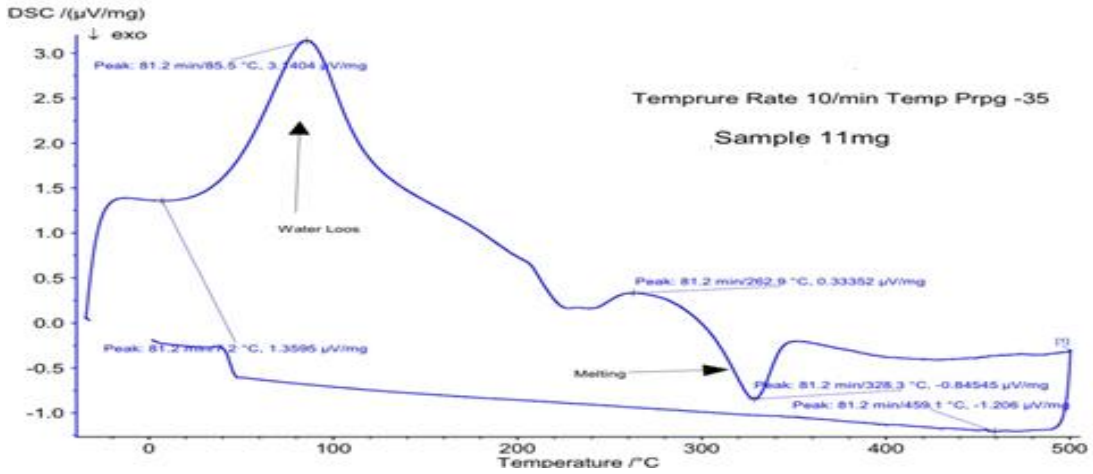

Figure 3.22: DSC curve of C-L_3 after extraction of Cu^{2+} from aqueous solution (pH 5).

3.4.1 Effect of pH:

Among chemical variables, pH is the most critical factor in solid-phase extraction (SPE). An optimal pH level minimizes matrix interference and enhances the effectiveness of the extraction process. To study the effect of pH on the extraction behavior of the sorbent material (C-L_3) toward Cu^{2+}, a 1 ppm Cu^{2+} solution was shaken with C-L_3 for 60 minutes over a pH range of 3.0 to 9.0.

A quantitative extraction (99.9%) was achieved at pH 5, with an adsorption capacity of 0.999 mg/g (Figures 3.23 and 3.24). Consequently, pH 5 was selected for further investigations.

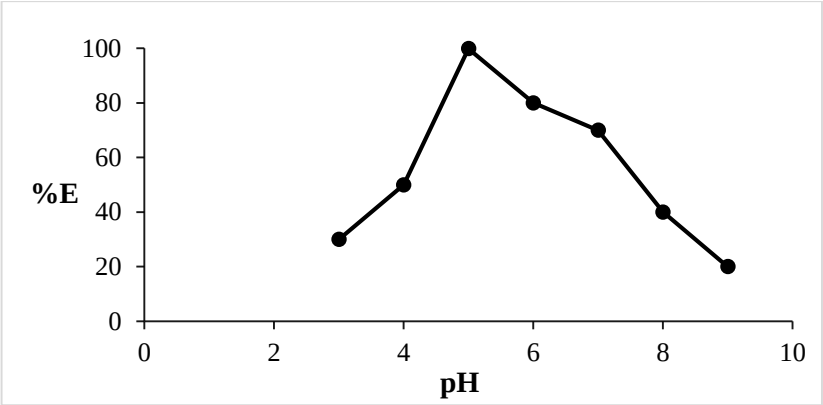

Figure 3.23: Study of the effect of pH on the extraction of Cu^{2+} (1 ppm) with C-L_3 (10 mg). Contact time 60 min.

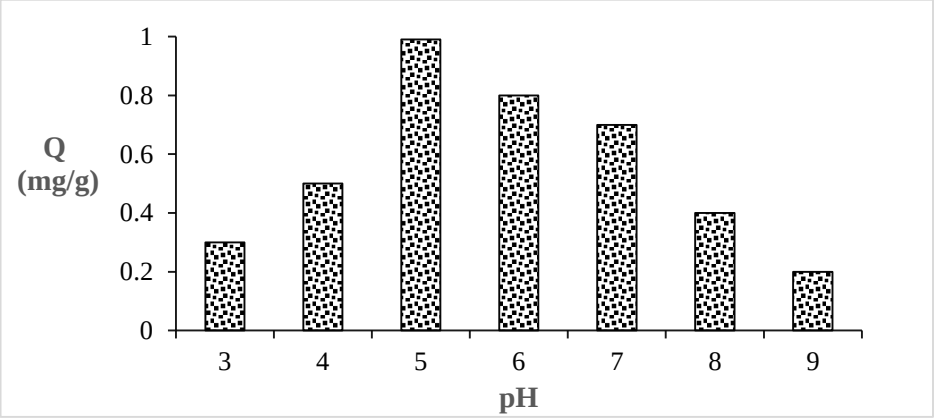

Figure 3.24: The effect of pH on the capacity of the adsorbent material on the extraction of Cu^{2+}

3.4.2 Effect of Contact Time:

Equilibrium time is a critical parameter in the batch extraction method. To determine the optimal contact time, a 1 ppm Cu^{2+} solution (pH 5) was shaken with 10 mg of C-L_3 for periods ranging from 1 to 90 minutes at room temperature. The adsorption capacity (Q) reached 0.999 mg/g after 5 minutes, with approximately 90% extraction efficiency achieved in this time (Figure 3.25). The high initial extraction rate is attributed to the availability of active ligand sites on the cellulose fiber. After 5 minutes, the extraction efficiency plateaued at 99.9%, with no significant changes observed upon further increases in contact time. Therefore, a contact time of 10 minutes was selected for further investigations.

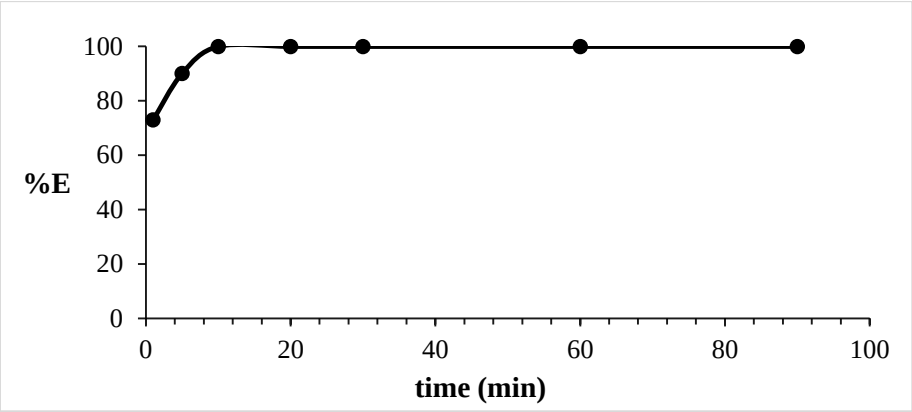

Figure 3.25: Effect of contact time on the extraction of Cu^{2+} (1 ppm) with C-L_3 (10 mg), pH 5.

3.4.3 Effect of Shaking Speed:

The experiment was conducted by shaking a 1 ppm Cu^{2+} solution (pH 5) with 10 mg of adsorbent (C-L_3) at shaking speeds ranging from 50 to 200 R/min for 10 minutes. Figure 3.26 illustrates the effect of shaking speed on the extraction efficiency. No significant impact of shaking speed on the extraction process was observed, as the adsorption capacity remained constant at 0.999 mg/g.

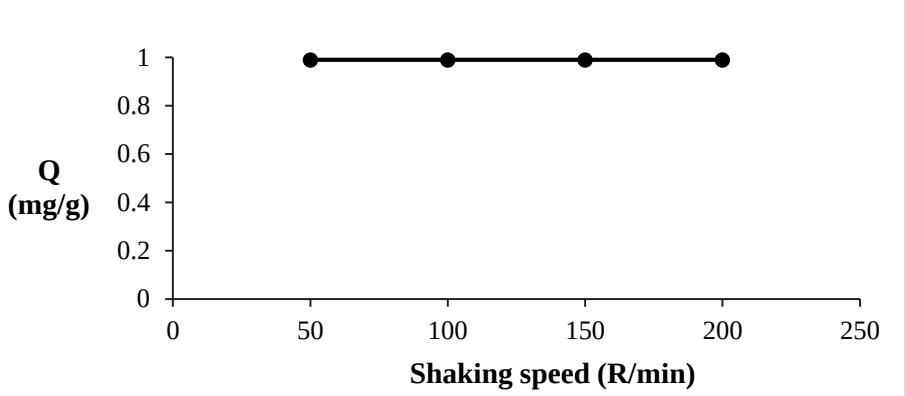

Figure 3.26: Effect of shaking speed on the extraction of Cu^{2+} with C-L_3 (10 mg), pH 5 and contact time of 10 min.

3.4.4 Effect of Ligand Concentration:

Initially, the extraction capability of free cellulose fiber (before ligand immobilization) toward Cu^{2+} was investigated. The cellulose fiber exhibited an adsorption capacity of 0.5 mg/g (Figure 3.27). However, this capacity doubled upon immobilization of L_3 on the cellulose fiber. To optimize the process, different ligand concentrations (0.5–22× 10^{-5} M) were immobilized on the cellulose fiber, and the extraction efficiency was evaluated

under the reported conditions (pH 5, 10 minutes). Results (Figure 3.27) demonstrated that all tested ligand concentrations achieved >95% extraction efficiency, with the 0.5×10^{-5} M concentration showing the highest performance. The adsorption capacity reached 0.999 mg/g, making this concentration the optimal choice for further studies.

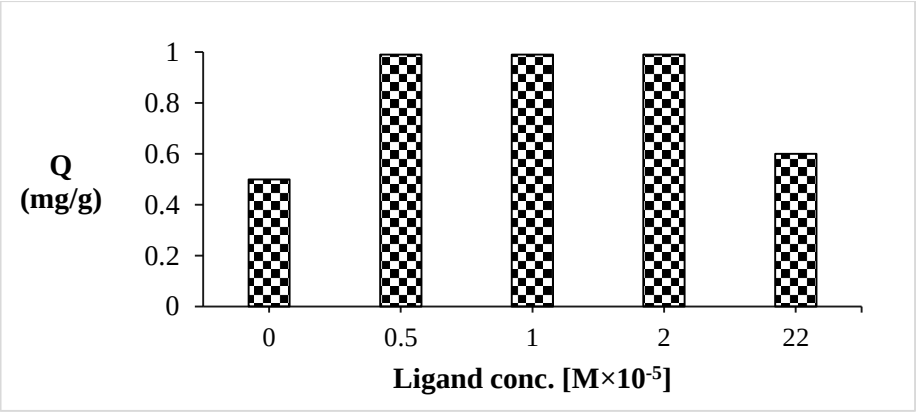

Figure 3.27: Effect of immobilized ligand (L_3) concentration on the Cu^{2+} (1 ppm) extraction using C-L_3 (10 mg), pH 5 and contact time 10 min.

3.4.5 Effect of Adsorbent Material Mass:

The effect of adsorbent mass on Cu^{2+} extraction was investigated using varying amounts of C-L_3 (5–500 mg). Results (Figure 3.28) showed that the amount of adsorbent had no significant impact on the extraction efficiency. The total adsorption capacity reached up to 1.8 mg/g, with 10 mg of adsorbent achieving 99.9% extraction efficiency. Therefore, 10 mg was selected as the optimal adsorbent mass for further studies.

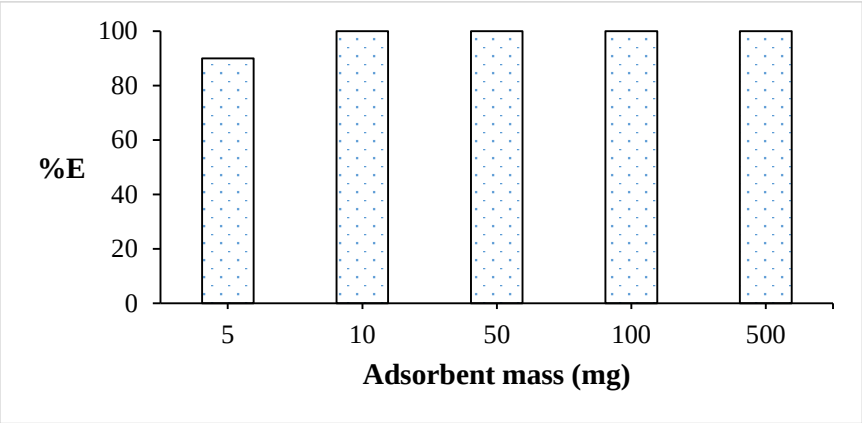

Figure 3.28: Effect of adsorbent material mass on the extraction, pH 5 and contact time 10 min.

3.4.6 Effect of Cu^{2+} Concentration:

The extraction capacity of the adsorbent material (C-L_3) was evaluated by studying its performance across a range of Cu^{2+} concentrations (0.05–100 ppm). The experiment involved shaking 10 mg of C-L_3 with the Cu^{2+} solutions for 10 minutes under optimal conditions. Figure 3.29 illustrates the effect of copper concentration on extraction efficiency. The adsorbent demonstrated excellent performance, achieving good extraction even at a low concentration of 0.05 ppm (50 ppb). The adsorption capacity (Q) increased with higher initial Cu^{2+} concentrations, as summarized in Table 3.10. This indicates that C-L_3 is highly effective for extracting trace amounts of Cu^{2+} from aqueous solutions, outperforming other sorbents [63]. A linear range with a slope of approximately 1.05 was observed (Figure 3.30). The distribution coefficient (D) was calculated using the following equation:

$$D = \frac{Q}{Ce} \quad \text{..... (4).}$$

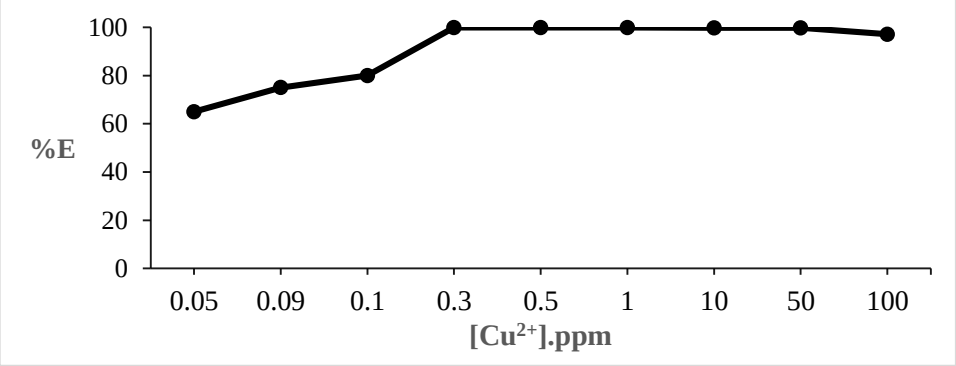

Figure 3.29: Effect of Cu^{2+} concentration on the extraction using C-L_3 (10 mg), pH 5 and contact time 10 min.

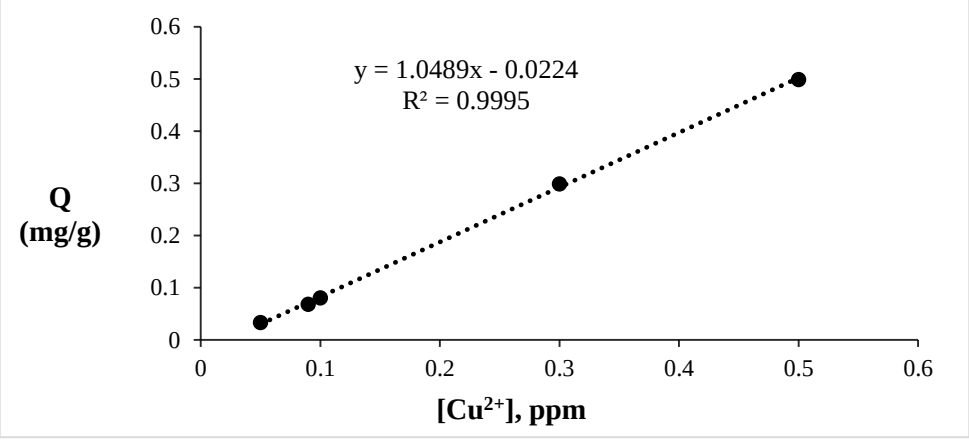

Figure 3.30: The dependence of the adsorbent capacity on Cu^{2+} concentration.

Table 3.10: Effect of Cu^{2+} concentration on the extraction using C-L_3 (10 mg), pH 5 and contact time 10 min conducted using batch method, n=3.

[Cu^{2+}], ppm	%E (±SD)	D	Capacity Q (mg g^{-1})
0.05	65 (0.42)	0.66	0.033
0.09	75 (0.42)	0.76	0.068
0.1	80 (0.58)	0.80	0.080
0.3	99.9 (0.07)	0.996	0.299
0.5	99.9 (0.07)	0.998	0.499
1.0	99.9 (0.07)	0.999	0.999
10.0	99.8 (0.15)	0.999	9.988
50.0	99.8 (0.15)	0.999	49.95
100	97.1 (0.1)	0.97	97.00

The distribution coefficient (D) for the total copper ion concentration (Cu^{2+}) in the adsorbent material (solid phase) was calculated from the plot of log D versus copper concentration (Figure 3.31). A unique ratio, with a slope of 1, was determined for the sum of the concentrations of all copper species adsorbed from the aqueous solution at pH 5.

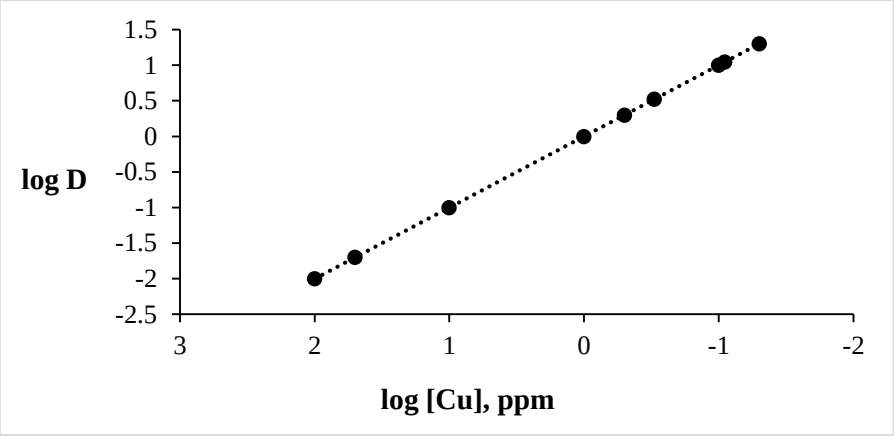

Figure 3.31: The dependence of the distribution on the metal ion concentration in used system

3.4.7 Effect of the Presence of Foreign Ions (Interferences):

To evaluate the selectivity of C-L_3 for Cu^{2+} extraction, the interactions with three foreign metal ions (Fe^{3+}, Ni^{2+}, and Pb^{2+}) were systematically analyzed. A 1 ppm Cu^{2+} solution was mixed with 0.5–2 ppm of each foreign metal ion and agitated with 10 mg of C-L_3 for 10 minutes. The concentration of extracted Cu^{2+} was then quantified. Table 3.11 shows that no significant interferences were observed for Ni^{2+} and Pb^{2+}. However, the presence of Fe^{3+} reduced the extraction efficiency of Cu^{2+} to 98% at a concentration of 2 ppm Fe^{3+}.

Table 3.11: Effect of metal ion interferences (Ni^{2+}, $Pb^{2+}$and Fe^{3+}) on the extraction of Cu^{2+} (1ppm) using C-L_3 (10 mg), pH 5 and contact time 10 min conducted using batch method. n =3.

Sample	Metal ion		Cu^{2+}	
	Type	Conc. ppm (added)	%E	Q (mg/g)
1	Ni^{+2}	0.5	99.9 (±0.07)	0.999
		0.8	99.9 (±0.07)	0.999
		1	99.9 (±0.07)	0.999
		2	99.9 (±0.07)	0.999
2	Pb^{+2}	0.5	99.9 (±0.07)	0.999
		0.8	99.9 (±0.07)	0.999
		1	99.9 (±0.07)	0.999
		2	99.9 (±0.07)	0.999
3	Fe^{+3}	0.5	99.9 (±0.07)	0.999
		0.8	99.5 (±0.44)	0.796
		1	99.5 (±0.44)	0.995
		2	98.1 (±0.01)	1.961

3.4.8 Reusability of the Sorbent:

The reusability of the C-L_3 sorbent was evaluated by conducting extraction-desorption experiments across three distinct extraction cycles in the acidic medium HCl (0.01-1 M). The extraction of Cu^{2+} consistently exceeded 99.9% across these three cycles (Figure 3.32). A clear drop was observed in the third cycle. This loss of reactivity of the sorbent could be due to the strong competition between protons and Cu^{2+} ions to occupy the ligand active sites, which might cause irreversible metal ion adsorption [52]. Table 3.12, summarized the optimum conditions for quantitative extraction of Cu^{2+} using the studied sorbent material.

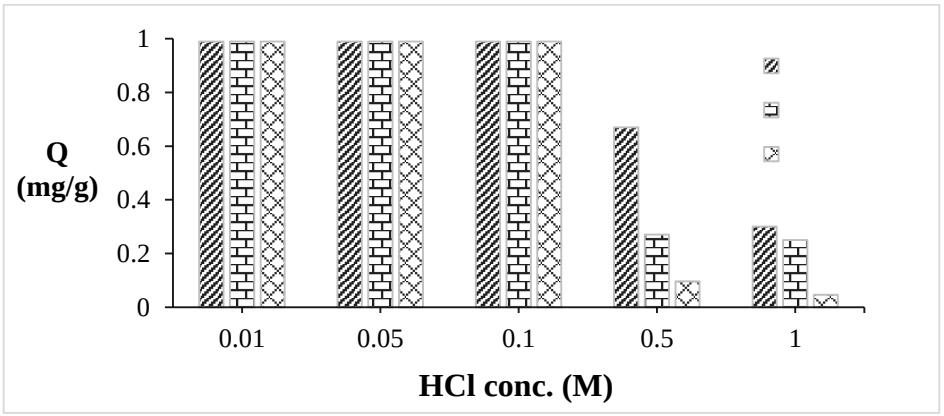

Figure 3.32: Reusability of the adsorbent (C-L_3) on the extraction of Cu^{2+}. n=3.

Table 3.12: Summary of the optimum parameters for the extraction of Cu^{2+} by C-L_3 sorbent.

Parameters	Condition
pH	5
Time	10 min
Shaken mechanically	50 R/min
Sorbent mass	10 mg
Cu^{2+}conc.	0.05-100 ppm
Ligand conc.	0.5×10^{-5} M
Capacity	0.999 mg/g

3.4.9 Preconcentration and Recovery of Cu^{2+} from Real Sample:

The efficiency of the adsorbent material (C-L_3) for Cu^{2+} extraction was evaluated using real samples under optimal conditions. Three water samples and two vegetable samples (tomatoes and potatoes) were tested. The two vegetables (tomatoes and potatoes) were purchased from the local market in Sirte City. The samples were first analyzed directly for their Cu^{2+} content using AAS. Results showed that Cu^{2+} was absent in all water samples, while the vegetables contained small amounts of Cu^{2+} (0.36 ppm in tomatoes and 0.87 ppm in potatoes). To assess the adsorbent's performance, 1 ppm Cu^{2+} was spiked into the water samples, and the extraction procedure was followed. A high recovery rate of 99.9% was achieved for water samples. However, the extraction efficiency for vegetables was lower compared to water samples. This reduction is likely due to the complex composition of vegetables, which includes proteins, fibers, and carbohydrates. These components can interact with Cu^{2+} to form complexes, reducing the availability of free Cu^{2+} for adsorption by C-L_3. This phenomenon is consistent with studies on metal adsorption and complexation in biological matrices [64]. Table 3.13 summarizes the recovery data obtained using the adopted procedure.

Table 3.13: Extraction Cu^{2+} from real sample pH 5, using batch method, n=3.

Sample		E %	(±SD)	Q (mg/g)
Chemistry lab, Faculty of Medicine.	S.1	99.9	0.07	0.999
Drinking water (SHIMA).	S.2	99.8	0.18	0.998
Water fountain in the downtown park.	S.3	99.9	0.07	0.999
Tomatoes (Vegetable market).	S.4	69.4	0.5	0.25
Potatoes (Vegetable market).	S.5	66.6	0.4	0.58

3.4.10 Isotherm Adsorption:

The adsorption curve (Figure 3.33) follows the L-type classification according to Giles, indicating that L_3 contains multiple polar functional groups (NO_2, C=N). These groups increase the effective surface area of the adsorbent, enhancing the number of active sites on the cellulose surface. This allows for the adsorption of a larger amount of the target material. The increased curvature intensity in the initial part of the curve reflects this behavior. Additionally, the polar groups in L_3 can form hydrogen bonds and van der Waals interactions with the adsorbed molecules, shifting the nature of the adsorption process from purely physical to partially chemical [65].

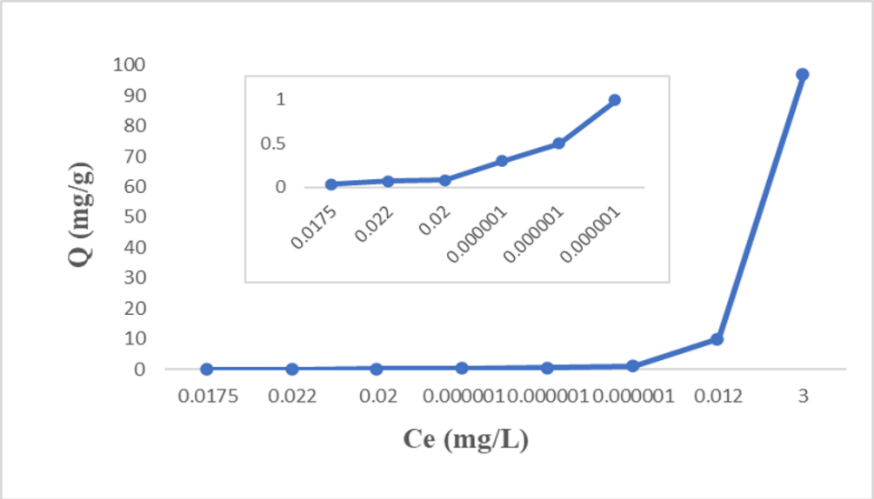

Figure 3.33: Adsorption isotherm curve.

3.4.10.1 Langmuir Equation:

The Langmuir equation was applied to the adsorption of copper from the aqueous medium onto the surface of C-L_3 at room temperature. From the slope and intercept plotted C_e vs C_e/q_e, the Langmuir constant was extracted as shown in the Figure 3.34, according to the following equation (5) [66]. Based on the results and the correlation coefficient values, it was concluded that the adsorption behavior does not conform to the Langmuir equation.

$$\frac{Ce}{Qe} = \frac{1}{aK} + \frac{Ce}{a} \quad \text{..... (5).}$$

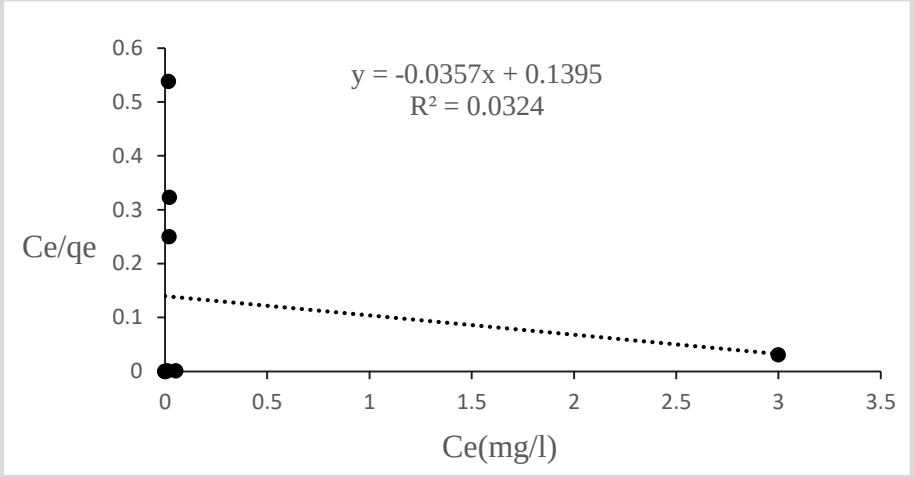

Figure 3.34: Adsorption isotherm Langmuir.

3.4.10.2 Freundlich Equation:

The Freundlich equation was applied to the adsorption of copper from the aqueous medium onto the surface of C-L_3 at room temperature. From the slope and intercept plotted ln C_e vs. ln q_e, the Freundlich constant was extracted as shown in the Figure 3.35 according to the following equation (6) [66]. Based on the results and the correlation coefficient values, it was concluded that the adsorption behavior does not conform to the Freundlich equation.

$$\ln Q_e = \ln K + \frac{1}{n} \ln C_e \text{..... (6).}$$

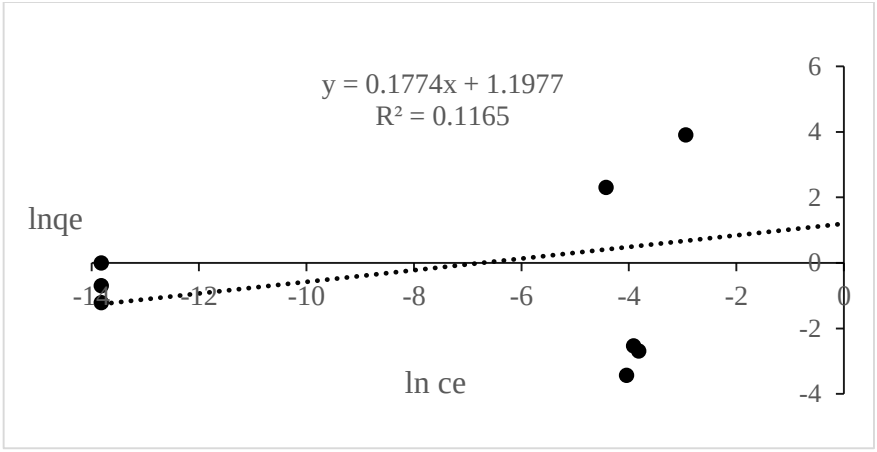

Figure 3.35: Adsorption isotherm Freundlich.

3.4.10.3 Temkin Equation:

The temkin equation was applied to the adsorption of copper from the aqueous medium onto the surface of C-L_3 at room temperature. From the slope and intercept plotted ln C_e vs q_e as shown in the (Figure 3.36). The temkin constants were extracted according to the following equation (7) [66].

$$Q_e = b_T \ln (K_T . C_e) \text{ ..…….. (7).}$$

Based on the results and the correlation coefficient values, it was concluded that the adsorption behavior conforms to the Temkin equation. The constants for the Temkin, Langmuir, and Freundlich models were extracted and are summarized in Table 3.14.

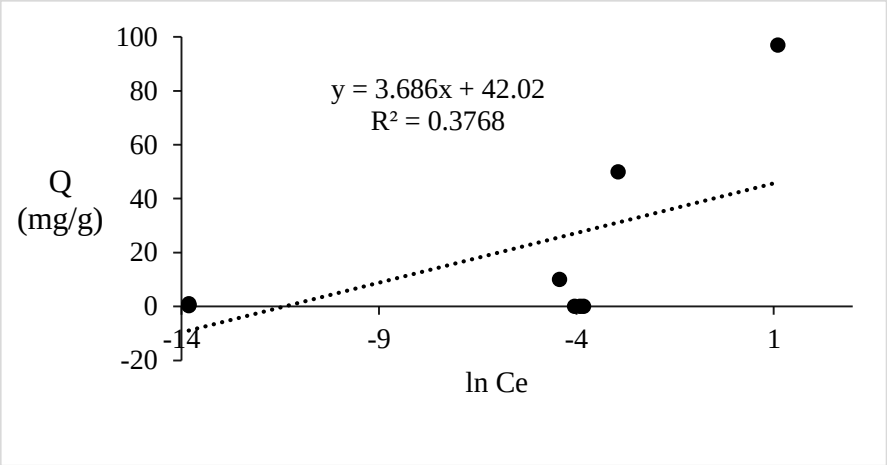

Figure 3.36: Adsorption isotherm Temkin.

Table 3.14: Langmuir, freundlich and temkin constants were extracted.

	Langmuir	**Frenudlich**	**Temkin**
Intercept	0.13953	1.1179	42.01956
Slope	-0.03569	0.1673	3.69
q_{max}	-28.03	-	-
K	-0.256	3.04	-
n	-	5.98	-
K_T	-	-	1.77×10^{18}
b_T	-	-	3.6

3.5 Adsorption Kinetic:

An equation was used to derive the adsorption rate constant of the C-L_3. Pseudo-second order equation (8) [67] was calculated (Table 3.15).

$$\frac{t}{qt} = \frac{1}{K2\ qe2} + \frac{t}{qe} \quad \text{..... (8).}$$

Where, t: time (min), q_t: adsorption amount at time, q_e: adsorption amount at equilibrium, K_2; pseudo-second order adsorption rate constant.

Table 3.15: Pseudo-second order adsorption rate constant.

Slope	Intercept	K_2 (M^{-1} min^{-1})
0.986	0.998	0.975

The adsorption kinetics of Cu^{2+} on the surface of C-L_3, and was carried out by shaking Cu^{2+} solution 50 R/min (1 ppm, pH 5) with 10 mg C-L_3. Results of the pseudo-second order adsorption kinetics was reported from a plot time vs t/q_t (Figure 3.37).

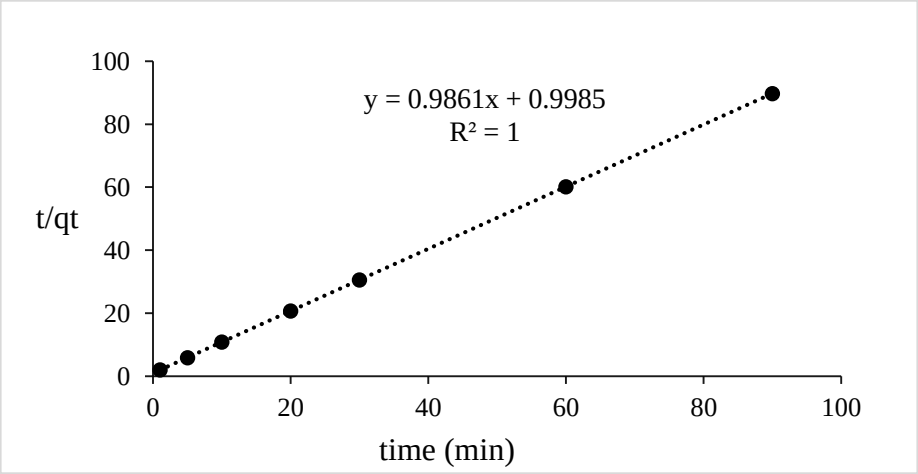

Figure 3.37: Pseudo-second order adsorption kinetics.

3.6 Comparison with Previous Studied:

The present method was compared with previously reported approaches for Cu^{2+} extraction from aqueous solutions. Table 3.16 summarizes some of the earlier studies on solid phase extraction (SPE) of Cu^{2+}. The sorption characteristics of the studied adsorbent material (C-L_3) are comparable to those of other SPE systems for Cu^{2+} extraction [52]. The current work demonstrates high selectivity and good adsorption capacity for Cu^{2+}, making it a promising alternative for extraction applications.

Table 3.16: Summary of some of the early reports on the solid phase extraction (SPE) of Cu^{2+}.

Ionophore (Support)	**Q (mg/g)**	**Time (min)**	**Reference**
Silica immobilized hydrazone compound.	0.054	90	[55]
Coconut fiber (coir) immobilized hydrazone compound.	2	25	[52]
Tannin-immobilized cellulose fiber extracted from coconut husk.	0.729	30	[68]
C-L_3.	0.999	10	Present work

Chapter 4

Conclusions and Recommendation for Future Work

4.1 Conclusions:

Hydrazone compounds are widely recognized for their biological and chemical properties, as well as their applications in various fields. One notable application is the extraction of metal ions using hydrazone compounds immobilized on selected sorbents. In this study, three novel hydrazone compounds 2,4-dinitrophenyl hydrazone acetophenone (DNPHACP), 2,4-dinitrophenyl hydrazone acetaldehyde (DNPHACT), and 2,4-dinitrophenyl hydrazone benzophenone (DNPHB) were successfully synthesized from three different starting materials. These compounds were characterized using FT-IR and DSC analysis. An adsorbent material was fabricated by immobilizing the synthesized hydrazone ligands on cellulose extracted from coconut fiber. The prepared material (C-L_3) exhibited higher thermal stability (>300 °C) compared to the free ligand (≤300 °C). C-L_3 demonstrated selective extraction of Cu^{2+} in a neutral medium, achieving 99.9% extraction efficiency using the batch method. The optimal conditions for solid-phase extraction (SPE) of Cu^{2+} from an acidic medium (pH 5) were determined to be 10 mg of C-L_3 at a ligand concentration of 0.5×10^{-5} M. The distribution coefficient (D) was found to be 0.999 mg/L. Adsorption kinetics followed a pseudo-second order model, confirming the efficiency of the process. This method is highly recommended for the selective removal of Cu^{2+} ions from water samples.

4.2 Recommendations for Future Work:

Although the results presented in this dissertation are complete, further work can be done to fulfill a complete information about the system. This include:

- Study of the interference of other heavy metal.
- Study of some other factors such as the temperature, etc.
- Study the other hydrazone ligands and their complexes with copper.
- Applying the method for the removal of copper from its samples.

References

1. Shah, M. A., Uddin, A., Shah, M. R., Ali, I., Ullah, R., Hannan, P. A., and Hussain, H. "Synthesis and characterization of novel hydrazone derivatives of isonicotinic hydrazide and their evaluation for antibacterial and cytotoxic potential." *Molecules* 27.19 (2022): 6770. https://doi.org/10.3390/molecules27196770.
2. Belskaya, Nataliya P., Wim Dehaen, and Vasiliy A. Bakulev. "Synthesis and properties of hydrazones bearing amide, thioamide and amidinfunctions." (2010):275-332. http://dx.doi.org/10.3998/ark.5550190.0011.108.
3. Pospieszna-Markiewicz, I., Fik-Jaskółka, M. A., Hnatejko, Z., Patroniak, V., and Kubicki, M. "Synthesis and Characterization of Lanthanide Metal Ion Complexes of New Polydentate Hydrazone Schiff Base Ligand." *Molecules* 27.23 (2022): 8390. https://doi.org/10.3390/molecules27238390.
4. Kumar, S. S., Sadasivan, V., Meena, S. S., Sreepriya, R. S., and Biju, S. "Synthesis, structural characterization and biological studies of Ni (II), Cu (II) and Fe (III) complexes of hydrazone derived from 2-(2-(2,2-dimethyl-4,6-dioxo-1,3-dioxan -5- ylidene) hydrazinyl) benzoic acid." *Inorganica Chimica Acta* 536 (2022): 120919.https://doi.org/10.1016/j.ica.2022.120919
5. Uchiyama, S., Kaneko, T., Tokunaga, H., Ando, M., and Otsubo, Y."Acid-catalyzed isomerization and decomposition of ketone-2,4-dinitrophenyl hydrazones" *Analytica chimica acta* 605.2 (2007): 198-204. https://doi. org/ 10.1016/j.aca. 2007.10.031.
6. Patel, Mittal M., and Mayur C. Shah. "Review on Spectrophotometric Method for Formation of Metal Complexes of Hydrazone Derivatives." http://ymerdigital.com.
7. Lgaz, H., Chung, I. M., Albayati, M. R., Chaouiki, A., Salghi, R., and Mohamed, S. K. "Improved corrosion resistance of mild steel in acidic solution by hydrazone derivatives: An experimental and computational study." *Arabian Journal of Chemistry* 13.1 (2020): 2934-2954.https://doi.org/10.1016 /j.arabjc.2018.08.004.
8. Aldib, Mohanad. *An investigation of the performance of photochromic dyes and their application to polyester and cotton fabrics*. Diss. Heriot-Watt University, 2013. http://hdl.handle.net/10399/2723.
9. Hussain, G., Akram, S., Lateef, M., Tanoli, A. K., Ali, N., and Khan, Z. "Hydrazone Ligand and Metal Complexes: A Comprehensive Study on Synthesis, Characterization, and Urease Inhibition Potential." *Journal of Population Therapeutics and Clinical Pharmacology* 31.2 (2024): 838-848.
10. Gup, R., and Emrah G. "Metal complexes and solvent extraction properties of isonitrosoacetophenone2-aminobenzoylhydrazone". *Spectrochimica Acta Part A: Molecular and Biomolecular Spectroscopy* 65.3-4 (2006): 719-726. https://doi.org /10.1016/j.saa.2006.01.004.
11. Das, S., and Samudranil P. "Copper (II) complexes with tridentate N-(benzoyl)-N′-(salicylidine)-hydrazine and monodentate N-heterocycles: Investigations of intermolecular interactions in the solid state." *Journal of molecular structure* 753.1-3 (2005): 68-79.

https://doi.org/10.1016/j.molstruc.2005.05.037.
12. Ravoof, T. and Bernhardt, P. "Synthesis, characterization and bioactivity of mixed-ligand Cu (II) complexes containing Schiff bases derived from S-benzyldithiocarbazate and saccharinate ligand and the X-ray crystal structure of the copper-saccharinate complex containing S-benzyl-β-N-(acetylpyrid-2-yl) methylenedithiocarbazate." *Polyhedron* 26.6 (2007): 1159-1165. https://doi.org/10.1016/j.poly.2006.03.007.
13. Bonardi, A., Ianelli, S., Pelizzi, C., Pelizzi, G., and Solinas, C "Copper (II), nickel (II) and iron (II) complexes of 2, 6-diacetylpyridine bis {[dl-hydroxy (phenyl) acetic] hydrazone}. X-ray structure of a 1: 2 metal: ligand nickel complex." *Inorganica chimica acta* 232.1-2 (1995): 211-216. https://doi.org/10.1016/0020-1693(94)04372-3.
14. Ekberg, C., Fermvik, A., Retegan, T., Skarnemark, G., Foreman, M. R. S., Hudson, M. J., and Nilsson, M. "An overview and historical look back at the solvent extraction using nitrogen donor ligands to extract and separate An (III) from Ln (III)." *Radiochimica Acta* 96.4-5 (2008): 225-233. https://doi.org/ 10.1524/ract. 2008.1483.
15. El-Behery, M., and Haifaa El-T. "Synthesis, magnetic, spectral, and antimicrobial studies of Cu (II), Ni (II) Co (II), Fe (III), and UO2 (II) complexes of a new Schiff base hydrazone derived from 7-chloro-4-hydrazinoquinoline." *Spectrochimica Acta Part A: Molecular and Biomolecular Spectroscopy* 66.1 (2007): 28-36. org/10.1016/j.saa.2006.02.017.
16. Wang, B. D., Yang, Z. Y., Crewdson, P., and Wang, D. Q. "Synthesis, crystal structure and DNA-binding studies of the Ln (III) complex with 6-hydroxychromone-3-carbaldehyde benzoyl hydrazone." *Journal of inorganic biochemistry* 101.10 (2007): 1492-1504. https://doi.org/10.1016/j.jinorgbio. 2007.04.007.
17. Jabeen, Mussarat. "A comprehensive review on analytical applications of hydrazone derivatives." *Journal of the Turkish Chemical Society Section A: Chemistry* 9.3 (2022): 663-698. https://doi.org/10.18596/jotcsa.1020357.
18. Fu, Fenglian, and Qi Wang. "Removal of heavy metal ions from wastewaters: a review." *Journal of environmental management* 92.3 (2011): 407-418. https://doi.org/10.1016/j.jenvman.2010.11.011.
19. Alum, E. "Highlights of heavy metals: Molecular toxicity mechanisms, exposure dynamics, and environmental presence". *Journal of Applied Sciences.* 10.3 (2023):8-19. https://doi.org/ 10.59298 /IAAJAS/2023/4.2.3222.
20. Wang, X., Ren, K., Jiao, K., Nie, W., An, X., and Lian, B."Selective immobilization of Pb (II) by biogenic whewellite and its mechanism." *Journal of Environmental Sciences* 137 (2024): 664-676. https://doi.org/10.1016/j.jes. 2023.03.014.
21. Rajendran, S., Priya, T. A. K., Khoo, K. S., Hoang, T. K., Ng, H. S., Munawaroh, H. S. H., and Show, P. L. "A critical review on various remediation approaches for heavy metal contaminants removal from contaminated soils." *Chemosphere* 287 (2022): 132369.https://doi.org/ 10.1016/j.chemosphere.2021.132369.

22. Selvi, A., Rajasekar, A., Theerthagiri, J., Ananthaselvam, A., Sathishkumar, K., Madhavan, J., and Rahman, P. K."Integrated remediation processes toward heavy metal removal/recovery from various environments-a review." *Frontiers in Environmental Science* 7 (2019):66. https://doi.org/10.3389/fenvs.2019.00066.
23. Ramezani, M., Enayati, M., Ramezani, M., and Ghorbani, A. "A study of different strategical views into heavy metal (oid) removal in the environment." *Arabian Journal of Geosciences* 14 (2021): 1-16. https://doi.org/10.1007/s12517-021-08572-4.
24. Sultana, M., Ahmmed, M. R., Ul Hoque, M. I., Ebna Mohsen, T., Mondal, A., Rahaman, M. H., and Alam, S. N. "Biodegradable Composite of Gelatin Blend Microcrystalline Cellulose for Cd^{2+}, Pb^{2+}, and Cr^{3+} Adsorption from an Aqueous Solution." *Advances in Polymer Technology* 2023.1 (2023): 1893660. https://doi.org/10.1155/2023/1893660.
25. Kalaiselvi, K., Mohandoss, S., Ahmad, N., Khan, M. R., and Manoharan, R. K."Adsorption of Pb^{2+} Ions from Aqueous Solution onto Porous Kappa-Carrageenan/Cellulose Hydrogels: Isotherm and Kinetics Study." *Sustainability* 15.12 (2023): 9534. https://doi.org/10.3390/su15129534.
26. Ibikunle, A. A., Ogunneye, A. L., Sanyaolu, N. O., Olutayo, K. A., Ogundare, S. A., Ogunmoye, A. O., and Moberuagba, K. H. "Application of modified cellulose for Pb^{2+} and Cu^{2+} removal from aqueous solutions: Kinetic and isotherms studies." *Scientia Africana* 22.1 (2023): 115-132. https://dx.doi.org/10 .4314/sa.v22i1.11.
27. Bennacer, L., Benmammar, D., Ahfir, N. D., Alem, A., Mignot, M., Pantet, A., and El Maana, S."Potential of using Alfa grass fibers (Stipa Tenacissima L.) to remove Pb^{2+}, Cu^{2+}, and Zn^{2+} from an aqueous solution." *Environmental Technology* 45.8 (2024): 1651-1667. https://doi.org/10.1080/09593330.2022.2148572.
28. Zaki, R. M., Setiabudi, H. D., Kamarudin, N. H. N., and Abdulkadir, B. A. "Adsorption of Pb (II) from Aqueous Solution Using Dendritic Fibrous Type SBA-15 (DFSBA-15)." *Journal of Chemical Engineering and Industrial Biotechnology* 8.2 (2022). https://doi.org/10.15282/jceib.v 8i2.8716.
29. Miretzky, P., and A. Fernandez C. "Cr (VI) and Cr (III) removal from aqueous solution by raw and modified lignocellulosic materials: a review." *Journal of hazardous materials* 180.1-3 (2010): 1-19. https://doi.org/10.1016/j.jhazmat.2010.04.060.
30. Cates, L. A., Cho, Y. M., Smith, L. K., Williams, L., and Lemke, T. L. "Phosphorus-nitrogen compounds. 20. Thiophosphorus hydrazones." *Journal of Medicinal Chemistry* 19.9 (1976): 1133-1137. https://pubs.acs.org/doi/abs/10.1021/jm00231a010.
31. Hyun, C., and Lucio J. F. "Inherited copper toxicosis with emphasis on copper toxicosis in Bedlington terriers." *Journal of Experimental Animal Science* 43.1 (2004): 39-64. https://doi.org/10.1016/j.jeas.2004. 01.003.
32. Haji Shabani, A. M., Dadfarnia, S., Nasirizadeh, N., and Shishehbore, M. R. "Preconcentration of copper with dithizone-naphthalene for subsequent

determination by atomicyng] absorption spectrometry." *Journal of Analytical Chemistry* 62 (2007): 46-50. https://doi.org/ 10.1134/S1061934807010108.

33. Tobiasz, A., and Stanisław W. "Solid-phase-extraction procedures for atomic spectrometry determination of copper." *TrAC Trends in Analytical Chemistry* 62 (2014): 106-122. https://doi.org/10.1016/j.trac.2014.06.018.
34. Kadadou, D., Tizani, L., Alsafar, H., and Hasan, S. W. "Analytical methods for determining environmental contaminants of concern in water and wastewater." *MethodsX* (2024): 102582. https://doi.org/10.1016/j.mex.2024.102582.
35. Mashhadizadeh, M. H., Pesteh, M., Talakesh, M., Sheikhshoaie, I., Ardakani, M. M., and Karimi, M. A. "Solid phase extraction of copper (II) by sorption on octadecyl silica membrane disk modified with a new Schiff base and determination with atomic absorption spectrometry." *Spectrochimica Acta Part B: Atomic Spectroscopy* 63.8 (2008): 885-888. https://doi.org/10.1016/j.sab.2008.03.018.
36. Soylak, M., and Omer E. "Selective separation and preconcentration of copper (II) in environmental samples by the solid phase extraction on multi-walled carbon nanotubes." *Journal of Hazardous Materials* 168.2-3 (2009): 1527-1531.
37. Diniz, K., Mariana G., and César R. "Synthesis and adsorption studies of novel hybrid mesoporous copolymer functionalized with protoporphyrin for batch and on-line solid-phase extraction of Cd^{2+} ions." *Reactive and Functional Polymers*73.6(2013):838-846. https://doi.org/10.1016/j.reactfunctpolym.2013.03.017.
38. Jolly, F., Md Z., and Zahida M. "Wastewater treatment using coconut fibre ash as an adsorbent for removal of heavy metals." *Archives of Agriculture and Environmental Science* 7.2 (2022): 192-198. https://doi.org/10.26832/24566632.2022.070207.
39. Ofomaja, A. E., Naidoo, E. B., and Modise, S. J. "Removal of copper (II) from aqueous solution by pine and base modified pine cone powder as biosorbent." *Journal of Hazardous Materials* 168.2-3 (2009): 909-917. https://doi.org/10.1016/j.jhazmat.2009.02.106.
40. Jha, S., Gaur, R., Shahabuddin, S., Ahmad, I., and Sridewi, N. "Kinetic and isothermal investigations on the use of low cost coconut fiber-polyaniline composites for the removal of chromium from wastewater." *Polymers* 14.20 (2022): 4264. https://doi.org/10.3390/polym 14204264.
41. Barbosa, R. B., Magriotis, Z. M., Gândara, A. P. A., Santiago, W. D., Alvarenga, G. F., Brandão, R. M., and Cardoso, M. D. G. "Kinetic, thermodynamic and physical-chemical study of the removal of copper from cachaça using coconut fibers." *Food Additives & Contaminants: Part A* 39.9 (2022): 1544-1554. https://doi.org/ 10.1080/19440049.2022.2096930.
42. Fritz, James S. "Analytical solid-phase extraction." *Analytical solid-phase extraction*. 1999. 209-209. ID: biblio-1074229.
43. Sakka, Sumio, ed. *Handbook of Sol-Gel Science and Technology: Processing, Characterization and Applications: Volume III. Applications of Sol-Gel Technology*. Springer, (2005).

44. علي الدجون. "الفاكهة المستديمة الخضرة." مكتبة مدبول. القاهرة. (1995).
45. The image was provided within an AI-generated response from OpenAI's ChatGPT for educational and illustrative use. (3/11/2024).
46. Poornachandhra, C., Jayabalakrishnan, R. M., Balasubramanian, G., Lakshmanan, A., Selvakumar, S., Maheswari, M., and John, J. E. "Coconut husk fiber: A low-cost bioresource for the synthesis of high-value nanocellulose." *Biointerface Research in Applied Chemistry* 13.6 (2023): 1-25.
47. Gupta, V. K., Carrott, P. J. M., Singh, R., Chaudhary, M., and Kushwaha, S."Cellulose: a review as natural, modified and activated carbon adsorbent." *Bioresource technology* 216 (2016): 1066-1076. https://doi.org/10.1016/j.biortech.2016.05.106.
48. del Río, J. C., Rencoret, J., Gutiérrez, A., Elder, T., Kim, H., and Ralph, J. "Lignin monomers from beyond the canonical monolignol biosynthetic pathway: another brick in the wall." *ACS Sustainable Chemistry & Engineering*, 8(13), (2020):4997-5012. Retrieved from pubs.acs.org/journal/ascecg.
49. Laine, C. "Structures of hemicelluloses and pectins in wood and pulp.Helsinki". University of Technology (*Espoo, Finland*), (2005):pp15-22.
50. Irawan, D., N. Muslimah, and Z. Arifin. "Lignin isolation from coconut coir with variation of time and concentration of NaOH in the process of alkaline delignification."*Chemical* 11.4 (2018): 1458-1460. http://www.rasayanjournal.co.in.
51. Connell, O., David W., Colin B., and Thomas O'D. "Heavy metal adsorbents prepared from the modification of cellulose: A review." *Bioresource technology* 99.15 (2008): 6709-6724. https://doi.org/10.1016/j .biortech.2008.01.036.
52. Ashraf M. A. Abdussalam S. M. A., and Abobaker E. A., Preliminary investigation on the extraction ability of hydrazine compounds immobilized on plant fibre towards Copper ions. *Journal of Science*, (2019), 8, 111-117.
53. برتيمة حكيمة، هركوس خضرة. "تحضير البلاستيك الحيوي من السيليلوز المستخلص من نخيل التمر." جامعة الشهيد حمة لخضر الوادي كلية التكنولوجيا. (2018).
54. Salhin, A., Tameem, A. A., Saad, B., Ng, S. L., and Fun, H. K. "4-Hydroxy-N′-[(E)-(2-hydroxyphenyl) methylidene] benzohydrazide." *Acta Crystallographica Section E: Structure Reports Online* 63.6 (2007): o2880-o2880. https://doi.org/10.1107/S1600536807021745.
55. Salhin, A., and Alshaqsi, S. "Preparation, characterization and utilization of immobilized1-((bromomethyl) (phenyl) ethyl)-2-(2, 4-dinitrophenyl) hydrazine for a study of solid phase extraction of copper ion cu (II). "(2011). Final year Project, School of Chemical Sciences University Sains Malaysia.
56. Miyazawa, M., Pavan, M. A., Muraoka, T., Carmo, C. A. F. S., and Melo, W. J. "Chemical analysis of plant tissues." *Manual of chemical analysis of soils, plants and fertilizers. Embrapa Informação Tecnológica, Brasília, DF, Brazil (in Portuguese)* (2009): 191-233.

57. Pavia, D. "Introduction to spectroscopy/Donald L." *Pavia, Gary M. Lampman, George S. Kriz, and James R. Vyvyan." SERBIULA (sistema Librum 2.0)* (2015).
58. Geschke, D., and K. Pöschel. "Dynamic processes in polymeric networks as studied by NMR relaxation methods." *Colloid and Polymer Science* 264 (1986): 482-487.
59. Feldman, D., and D. D. S. C. Banu. "DSC analysis for the evaluation of an energy storing wallboard." *Thermochimica acta* 272 (1996): 243-251. https://doi.org/ 10.1016/0040- 6031(95)02456-5.
60. Bari, F., Begum, N., Jamaludin, S. B., and Hussin, K. "Extraction and separation of Cu (II), Ni (II) and Zn (II) by sol–gel silica immobilized with Cyanex 272." *Hydrometallurgy* 96.1-2 (2009): 140-147. https://doi.org/10.1016/j.hydromet. 2008.09.006.
61. Sadeghi, S., and Sheikhzadeh, E. "Solid phase extraction using silica gel modified with murexide for preconcentration of uranium (VI) ions from water samples." *Journal of Hazardous Materials* 163.2-3 (2009): 861-868. https://doi.org/10 .1016/j.jhazmat.2008.07.053.
62. Li, C., Pan, J., Zou, X., Gao, J., Xie, J., and Yongsheng, Y. "Synthesis and applications of novel attapulgite-supported Co (II)-imprinted polymers for selective solid-phase extraction of cobalt (II) from aqueous solutions." *International Journal of Environmental Analytical Chemistry* 91.11 (2011): 1035-1049. https://doi.org/10.1080/03067310903502752.
63. Saad, B., Chong, C. C., Ali, A. S. M., Bari, M. F., Ab Rahman, I. Mohamad, N., and Saleh, M. I. "Selective removal of heavy metal ions using sol–gel immobilized and SPE-coated thiacrown ethers." *Analytica chimica acta* 555.1 (2006): 146-156. https://doi.org/10.1016/j.aca.2005.08.070.
64. Balabanova, B., Stafilov, T., Bačeva, K., and Vučković, I. "Heavy metals toxicity and bioaccumulation in vegetables from potentially polluted area." *Scientific Works of the Agricultural University-Plovdiv, 60, 615–620 (2013)* (2013).
65. CH, GILES. "Studies in adsorption. Part XI. A system of classification of solution adsorption isotherms, and its use in diagnosis of adsorption mechanisms and in measurements of specific surface areas of solids." *J. Chem. Soc.* 786 (1960): 3973-3993.
66. توفيق، إ. م. دراسة قابلية وحركية امتزاز بعض الصبغات العضوية على سطح مسحوق الصخور السليسية العراقية. رسالة ماجستير، كلية التربية للعلوم الصرفة / ابن الهيثم، جامعة بغداد، 2019. مخطوطة غير منشورة، 120 صفحة.
67. Simonin, Jean-Pierre. "On the comparison of pseudo-first order and pseudo-second order rate laws in the modeling of adsorption kinetics." *Chemical Engineering Journal* 300 (2016): 254-263. https://doi.org/10.1016/j.ce .2016. 04.079.
68. Taksitta, K., Sujarit, P., Ratanawimarnwong, N., Donpudsa, S., and Songsrirote, K. "Development of tannin-immobilized cellulose fiber extracted from coconut husk and the application as a biosorbent to remove heavy metal ions."

Environmental Nanotechnology, Monitoring & Management 14 (2020): 100389. https://doi.org/10.1016/j.enmm.2020.100389.

الملخص

في هذا العمل تم إخضـــاع 4,2-ثنـائي فينيل الهيدرازين لتفـاعل التكثيف مع الأســـيتوفينون والأسـيتالدهيد والبنزوفينون مما أدى إلى إنتاج ثلاث من مركبات الهيدرازون، نتج عنه الحصـول على ثلاثة مركبات بنسـب مرضـية بلغت 75٪، 57٪، 85٪ على التوالي. تم تحضـير مادة مازة تعتمد على مركبات الهيدرازون المحضـرة عن طريق تثبيت هذه المركبات على الياف السـليلوز المستخرج من ثمار جوز الهند بنسبة 24.5٪ (4.9 جم). تمت بعدها دراسة قدرة المادة المازة على استخلاص النحاس بطريقة استخلاص الطور الثابت. أجريت التحاليل بواسطة جهاز الامتصـاص الذري. تم استخدام السليلوز المثبت كمرحلة ثابتة في الاستخلاص بالطور الصلب لاستخلاص أيون النحاس من المحلول المائي للنحاس الثنائي. تم تحديد الظروف المثلى للاستخلاص الفعال مثل الرقم الهيدروجيني ووقت التلامس وتركيز مركبات على الياف الســـيليلوز. أظهرت النتائج التي تم الحصـول عليها أن المادة الماصـة المدروسـة أظهرت انتقائية تفضـيلية تجاه النحاس الثنائي مقارنة بغيرها من المعادن الانتقالية المدروســة. تم اختبار الطريقة لاســتخلاص أيون النحاس الثنائي من العينات الحقيقية. تم العثور على نسبة استرداد (>60%).

PUBLICATIONS

Utilizing a Cost-Effective Adsorbent Material Derived from Coconut Coir Fiber Modified with Hydrazone Compounds for Efficient Removal of Copper from Aqueous Environments

Salwa Amer Belgasem and Abdussalam Salhin Mohamad*
Department of Chemistry, Faculty of Science, Sirte University
*Corresponding author: salam_salhin@su.edu.ly

Submission data: 25/1/2025 Electronic publishing data: 28/2/2025

Abstract: A hydrazone compounds derived from the condensation of 2,4-dinitrophenyl hydrazine with acetophenone, acetaldehyde, and benzophenone, were synthesized and their selectivity towards transition metal ions were investigated. The ligands were isolated in satisfactory yield of 75 %, 57 % and 85 % respectively. Sorbent material based on these hydrazone compounds was prepared by immobilizing the ligands into a cellulose extracted from coconut fibre. The capability of the sorbent material for the extraction of copper was studied by the batch method. The immobilized cellulose was used as a stationary phase in the solid phase extraction to extract Cu^{2+} ions from aqueous solution. The optimum condition for an effective extraction such as pH, contact time, Cu^{2+} and ligands concentrations were investigated. Results obtained showed that the studied sorbent exhibited preferential selectivity towards Cu^{2+} over other transition metals studied. The method was tested for the extraction of Cu^{2+} ions from real samples. Reasonable recovery (> 60 %) was found.

Keywords: Hydrazone compounds; Cellulose fibre; Solid phase extraction; Metal ions

Introduction:

Hydrazone derivatives have been used in the synthesis of metal complexes that exhibit a variety of geometrical configurations and magnetic properties, expanding their applicability across multiple scientific fields. The careful structural elucidation of these compounds and their derivatives is crucial for fully understanding their biological activities and therapeutic potential [1]. A prominent compound often employed in this area is 2,4-dinitrophenylhydrazine (DNPH) [2]. Hydrazones have the ability to form a wide range of chromophoric complexes with transition metals [3, 4]. The regulation of heavy metals poses a significant challenge due to their persistence and resilience in environmental matrices [5]. The cations Pb^{2+}, Cd^{2+}, Cu^{2+}, and Hg^{2+} are categorized as hazardous heavy metals, known for their harmful effects on both ecosystems and living organisms. Numerous research efforts have explored effective methods for the removal and remediation of heavy metals [6-9]. Adsorption of these metallic ions from aqueous solutions using various adsorbents, such as modified plant fiber and gelatin composite [10], kappa-carrageenan/cellulose hydrogel [11], acrylamide-grafted kola-nut pod husk cellulose [12], Alfa grass fibers [13], dendritic fibrous materials [14], has shown promising results in heavy metal extraction [15]. The extensive application of copper in industrial manufacturing processes may lead to increased copper concentrations in the environment. Nonetheless, heightened levels of Cu^{2+} present considerable risks to both ecological stability and human health. Elevated concentrations can cause substantial harm to vital organs, including the liver, erythrocytes, heart, and brain [16]. The process of extracting copper from environmental samples utilizes various advanced techniques, each offering unique benefits. These methodologies are essential for assessing contamination levels and safeguarding environmental integrity. Prominent extraction techniques employed in this research include solid-phase extraction (SPE) [17]. The SPE methodology has garnered substantial acclaim within the domain of analytical chemistry as a proficient pre-concentration technique for the isolation of trace metals [18]. The preference for utilizing SPE to extract heavy metal ions from aqueous matrices is predominantly attributed to its operational ease, absence of contaminants, elevated enrichment potential, effective phase separation, temporal efficiency, and economic viability [19]. The effectiveness of this methodology depends on the properties of the adsorbent, particularly regarding selectivity, detectability, sample throughput, and reusability [20]. The batch methodology is employed as a solid-phase extraction (SPE) technique, wherein a solid phase is used as an extractant to isolate a specific analyte from a given solution. Thereafter, the solid material may either be subjected to immediate analytical procedures or undergo an elution process for the recovery of the analyte [21]. Generally, a specific selective component is attached to a solid support, such as silica, alumina, titanium dioxide, or a polymer, which functions as the solid phase in the batch methodology [22]. Fibrous materials have exhibited significant adsorption capabilities across a diverse array of applications. Research has explored the adsorption efficacy of botanical fibers on various ions, indicating enhanced performance following chemical modification [23]. Agricultural residues consist of lignocellulosic components, primarily cellulose, hemicellulose, and lignin [24]. The sorption capacity of lignocellulosic waste is comparable to that of other natural sorbents while also providing advantageous characteristics such as minimal to no cost, high accessibility, and a straightforward operational methodology. Coir fiber has been extensively studied for its potential as an adsorbent in the removal of various metal ions from water. The husk of the coconut is a byproduct that constitutes the mesocarp of the coconut and represents approximately 33-35% of the whole husk. The cellulose, hemicellulose, lignin,

جامعة سرت
كلية العلوم
قسم الكيمياء

استخدام مادة ماصة فعالة من حيث التكلفة مشتقة من الياف جوز الهند المعدلة بمركبات هيدرازون لإزالة بعض المعادن الثقيلة بكفاءة من البيئات المائية.

إعداد الطالبة:

سلوى عامر بلقاسم سالم

تحت إشراف:

أ.د. عبد السلام الصالحين

قدمت هذه الرسالة كأحد متطلبات الحصول على درجة الإجازة العالية (الماجستير)

في العلوم تخصص الكيمياء

للعام الجامعي 2025/2024